



HAL
open science

Morphology of positive ionization waves in atmospheric pressure air: influence of electrode set-up geometry

Anne Bourdon, François Péchereau, Fabien Tholin, Zdenek Bonaventura

► To cite this version:

Anne Bourdon, François Péchereau, Fabien Tholin, Zdenek Bonaventura. Morphology of positive ionization waves in atmospheric pressure air: influence of electrode set-up geometry. *Plasma Sources Science and Technology*, 2021, 30 (10), pp.105022. 10.1088/1361-6595/ac2be5 . hal-03416799

HAL Id: hal-03416799

<https://hal.science/hal-03416799>

Submitted on 5 Nov 2021

HAL is a multi-disciplinary open access archive for the deposit and dissemination of scientific research documents, whether they are published or not. The documents may come from teaching and research institutions in France or abroad, or from public or private research centers.

L'archive ouverte pluridisciplinaire **HAL**, est destinée au dépôt et à la diffusion de documents scientifiques de niveau recherche, publiés ou non, émanant des établissements d'enseignement et de recherche français ou étrangers, des laboratoires publics ou privés.

ACCEPTED MANUSCRIPT

Morphology of positive ionization waves in atmospheric pressure air: influence of electrode set-up geometry

To cite this article before publication: Anne Bourdon *et al* 2021 *Plasma Sources Sci. Technol.* in press <https://doi.org/10.1088/1361-6595/ac2be5>

Manuscript version: Accepted Manuscript

Accepted Manuscript is “the version of the article accepted for publication including all changes made as a result of the peer review process, and which may also include the addition to the article by IOP Publishing of a header, an article ID, a cover sheet and/or an ‘Accepted Manuscript’ watermark, but excluding any other editing, typesetting or other changes made by IOP Publishing and/or its licensors”

This Accepted Manuscript is © 2021 IOP Publishing Ltd.

During the embargo period (the 12 month period from the publication of the Version of Record of this article), the Accepted Manuscript is fully protected by copyright and cannot be reused or reposted elsewhere.

As the Version of Record of this article is going to be / has been published on a subscription basis, this Accepted Manuscript is available for reuse under a CC BY-NC-ND 3.0 licence after the 12 month embargo period.

After the embargo period, everyone is permitted to use copy and redistribute this article for non-commercial purposes only, provided that they adhere to all the terms of the licence <https://creativecommons.org/licenses/by-nc-nd/3.0>

Although reasonable endeavours have been taken to obtain all necessary permissions from third parties to include their copyrighted content within this article, their full citation and copyright line may not be present in this Accepted Manuscript version. Before using any content from this article, please refer to the Version of Record on IOPscience once published for full citation and copyright details, as permissions will likely be required. All third party content is fully copyright protected, unless specifically stated otherwise in the figure caption in the Version of Record.

View the [article online](#) for updates and enhancements.

Morphology of positive ionization waves in atmospheric pressure air: influence of electrode set-up geometry

Anne Bourdon¹, François Péchereau², Fabien Tholin² and Zdenek Bonaventura³

¹ Laboratoire de Physique des Plasmas (LPP), CNRS, Sorbonne Université, Ecole Polytechnique, Institut Polytechnique de Paris, 91120 Palaiseau, France

² ONERA, 6, chemin de la Vauve aux Granges, 91123 Palaiseau, France

³ Faculty of Science, Masaryk University, Brno, Czech Republic

E-mail: anne.bourdon@lpp.polytechnique.fr

28 September 2021

Abstract. A numerical parametric study on positive diffuse discharges in point-to-plane geometry in air at atmospheric pressure is presented. Different discharge characteristics are studied: ignition time, connection time to the grounded cathode plane, shape of the discharge and its maximum radius at the connection time, evolution of the maximum electric field in the discharge front and velocity of the ionization front during its propagation. First, a case at a DC voltage of 50 kV applied on a rod anode ended by a semi-sphere with a radius of 100 μm set at 1.6 cm from a grounded cathode plane is considered. The influence of the rod radius, the position of a disc holder, the shape of the anode electrode and the radial extension of the computational domain are studied. The radius of curvature of the anode tip (varied between 100 and 1000 μm) and the shape of the anode electrode (rod or hyperbola) are shown to have a negligible influence on discharge characteristics. Conversely, the presence of a disc holder or a small radial computational domain lead to a decrease of the maximum discharge radius at the connection time and a change in the discharge shape from a conical to an ellipsoidal shape. These changes on the discharge morphology have only a limited impact on the propagation velocity of the discharge front and maximum electric field on the discharge axis. Then, a point-to-plane geometry with a rod electrode of 50 μm radius, in a 1.6 cm gap, with a 100 kV voltage applied with a rise time of 1 ns is studied. The influence of a disc holder on the discharge characteristics is the same as for lower DC voltages. Finally, the time evolution of the absolute value of the electric field at different test points on the discharge axis is studied. Close to the anode tip, rapidly after the peak of electric field due to the passage of the ionization front, the electric field in the discharge channel is shown to increase to values higher than the breakdown field.

Keywords: nanosecond discharge in air at atmospheric pressure, ionization wave dynamics, fluid simulation

Submitted to: *Plasma Sources Sci. Technol.*

1. Introduction

Recently, several experimental and numerical studies in point-to-plane geometry in air gaps of about 1 cm at atmospheric pressure have reported images of axisymmetric diffuse discharges with maximum radius of several centimeters as reviewed in Naidis et al. (2018) and shown since then in Brisset et al. (2019); Chng et al. (2019); Tarasenko et al. (2020); Tarasenko (2020); Chen et al. (2020); Bourdon et al. (2020); Babaeva and Naidis (2021); Zhu et al. (2021). These discharges are obtained using high voltage pulses (with maximum voltages being five or ten times higher than classical steady-state breakdown levels) applied with sub-nanosecond and nanosecond rise times. For both positive and negative polarities of the applied voltage at the point electrode, these diffuse discharges are shown to be formed due to an ionization wave propagating from the point electrode to the grounded plane (Naidis et al., 2018). For negative subnanosecond discharges, the effective generation of runaway electron beams near the point electrode has been reported experimentally (Naidis et al., 2018; Tarasenko, 2020). Results of simulations (Babaeva et al., 2018; Tarasenko et al., 2020) show an increase of the negative front velocity with this additional source of precursor electrons ahead of the discharge front. On the other hand, in positive polarity a diffuse-like discharge has been observed in certain electrode set-ups, while no x-rays nor runaways were detected (Brisset et al., 2019; Chng et al., 2019). Then, the understanding of conditions in which a diffuse nanosecond positive ionization wave can be obtained in atmospheric pressure air is of particular interest.

So far, the number of experimental and numerical studies on positive diffuse discharges in atmospheric pressure air remains limited (Naidis et al., 2018; Tardiveau et al., 2009; Pechereau et al., 2014; Babaeva and Naidis, 2016b; Babaeva and Naidis, 2016a; Marode et al., 2016; Tardiveau et al., 2016; Tarasenko et al., 2020; Chen et al., 2020; Bourdon et al., 2020; Babaeva and Naidis, 2021; Zhu et al., 2021). Rather good agreement between experiments and simulations has been obtained on discharge characteristics such as the maximum discharge radius and ionization front velocity as reviewed in Naidis et al. (2018); Babaeva and Naidis (2021) and on the time evolutions of the electric field on the symmetry axis as shown at very early times of discharge propagation in Brisset et al. (2019) and during the whole discharge propagation in the gap in Bourdon et al. (2020); Zhu et al. (2021).

As demonstrated for plasma jets in Xiong et al. (2012); Lietz and Kushner (2018), the geometry of electrodes and the location of grounded surfaces around the studied set-up has a major influence on discharges at atmospheric pressure. It is interesting to note that in experiments on diffuse discharges in point-to-plane geometry, different shapes and lengths of high voltage point electrodes are used, but in all cases, the radius of curvature of its tip is small, varying between 10 and 200 μm (with base values of 75 μm used in Tarasenko et al. (2018, 2020) and 50-100 μm used in Brisset et al. (2019); Chng et al. (2019)). Experimentally, Tardiveau et al. (2016) have studied the influence of the tip radius in the range 10 to 200 μm on the discharge characteristics and have reported only

Morphology of positive ionization waves ...

3

a small influence on discharge morphology and time development. In most simulation works, simple shapes of point electrodes are used (sphere in Babaeva and Naidis (2016b); Babaeva and Naidis (2016a), rod ended by semi-sphere in Bourdon et al. (2020), conical shape ended by a semi-sphere in Pechereau et al. (2014), parabolic shape in Marode et al. (2016); Brisset et al. (2019) and conical shape ended by a hyperboloid electrode in Chen et al. (2020)). Recently, in Zhu et al. (2021), a more complex shape (combining a conical pin with a metal cylinder on a trapezoidal holder) has been considered to be as close as possible to experiments in Chng et al. (2019). It is interesting to note that in numerical studies of positive diffuse discharges, the radius of curvature of the tip varies between $50 \mu\text{m}$ for Pechereau et al. (2014); Marode et al. (2016); Chen et al. (2020); Zhu et al. (2021) to $100 \mu\text{m}$ in Bourdon et al. (2020); Zhu et al. (2021) and between 1 to 5 mm in Tarasenko et al. (2020); Babaeva and Naidis (2016a); Babaeva and Naidis (2016b). In the simulations presented in Tarasenko et al. (2020), the sphere radius is varied between 1 and 1.5 mm for a constant DC applied voltage. It is shown that the influence of the tip radius on the average propagation velocity of the diffuse ionization wave is negligible. During the discharge propagation, the velocity is shown to vary significantly in the gap and is the highest close to the sphere electrode with the smallest radius. In the simulations presented in Zhu et al. (2021), it is mentioned that varying the curvature radius of the pin tip from 50 to $100 \mu\text{m}$ has also a negligible influence on the discharge evolution. Conversely, using three different shapes of the pin (close to experiment, elliptical and triangular), it is shown that the shape of the pin affects the calculated discharge morphology.

In experiments, to prevent parasite discharges that may happen due to the very high voltages used, holders of the high voltage point anode electrode have to be designed carefully as shown in set-up schemes in Tardiveau et al. (2016); Tarasenko et al. (2020). In diffuse discharge simulations with simple point electrode geometries, as in Naidis et al. (2018); Bourdon et al. (2020), no point holder is considered. In Bourdon et al. (2020) a weak radial discharge propagating around the cylindrical part of the rod electrode is observed. This radial discharge is much slower than the main axial positive diffuse ionization wave propagating from the tip to the grounded cathode plane. In Marode et al. (2016), a disc at the same voltage as the point electrode is set at 1 cm from the tip of a parabolic point electrode and no parasite discharges are observed. With a more complex shape of the high voltage point electrode, and in particular when sharp corners are present close to the tip, parasite radial discharges may become more intense as observed in the simulations carried out in Chen et al. (2020); Zhu et al. (2021). Finally, it is interesting to note that in experiments, the point-to-plane set-ups are usually set in a grounded metallic reactor. In simulations carried out so far on positive diffuse discharges, the influence of radial boundary conditions for electric potential on the characteristics of diffuse discharges has not been studied. It is interesting to note that the size of the radial computational domain varies from 1 cm in Marode et al. (2016) to 7.5 cm in Bourdon et al. (2020).

The objective of this work is to carry out a detailed parametric numerical study on

Morphology of positive ionization waves ...

4

the influence of the tip radius, the shape of the point anode electrode, the presence of a holder of the point anode electrode and the radial extension of the computational domain on the propagation velocity, peak electric field on the axis and maximum discharge radius of a positive ionization front propagating between a high voltage point anode electrode and a grounded cathode plane. In this work, the gap is fixed to 1.6 cm. This study is not intended to make side-by-side comparison to the results of any single experiment. Rather, in this study, we use the flexibility of numerical simulations to study separately the effects of several geometrical parameters that can not be decoupled easily in experiments. However, throughout the following sections, comparisons are made to experimental data for similar devices.

The model is described in section 2, and the results of our investigation are discussed in section 3. In section 3.1, the base case is a point-to-plane geometry with a DC applied voltage of 50 kV. The influence of the tip radius, presence and position of a disc as point holder, shape of the high voltage point electrode and radial extension of the computational domain are discussed. Then, in section 3.2, the influence of a disc as point holder on the discharge characteristics is studied for a higher voltage of 100 kV applied with a rise time of 1 ns. Finally, the time evolution of the electric field at different test points of the gap for the high voltage case of section 3.2 is discussed. Concluding remarks are in section 4.

2. Model formulation

The studied configuration is a point-to-plane geometry with a positive high voltage applied to a point electrode set at a distance $d_g = 1.6$ cm from a grounded plane as shown in Figure 1. As discussed in Naidis et al. (2018); Zhu et al. (2021), a classical fluid model can be used to simulate propagation of positive ionization fronts produced by subnanosecond high overvoltages. In this work, we use the same fluid model as in Bourdon et al. (2020), based on drift-diffusion equations for electrons, positive and negative ions coupled with Poisson's equation. As the discharge is axisymmetric, cylindrical coordinates (x, r) are used as shown in Figure 1.

In section 3.1, a DC voltage of 50 kV is applied to the point electrode which is, as a base case in this section, a rod of radius $R_r = 100$ μm ended by a semi-sphere with the same radius. Then, in the following, changing the radius of the rod electrode means changing both the radius of the rod and the radius of the semi-sphere at the tip, such that they always equal each other. In all the computations in section 3.1, the domain is a cartesian grid of size $R_d \times L$, where R_d is the position of the radial boundary, and L the extension of the domain in the axial direction (x), which is the sum of the gap distance d_g , and the distance d_p from the tip of the point to the disc holder or to the axial boundary of the computational domain (Figure 1). For the reference computational domain, we have considered as in Bourdon et al. (2020) $R_d = 7.52$ cm, and $d_p = 1$ cm, hence $L = d_g + d_p = 2.6$ cm. The reference grid used in this work is the same as in Bourdon et al. (2020) with $n_x \times n_r = 7252 \times 2400$. In section 3.1.1, the radius R_r of the rod and

semi-sphere is varied between 100 and 1000 μm . In section 3.1.2 a disc with the same applied voltage as the point electrode is set as holder at different distances d_p from the tip, as defined on Figure 1. The value of d_p is varied between 0.6 to 4.8 cm, keeping the same gap distance d_g , and results are compared with the base case without disc holder. For $d_p \geq 1$ cm, the grid is extended axially with a constant mesh size of 90 μm , which is the value of the mesh size at $d_p = 1$ cm in the reference grid. In Section 3.1.3, a

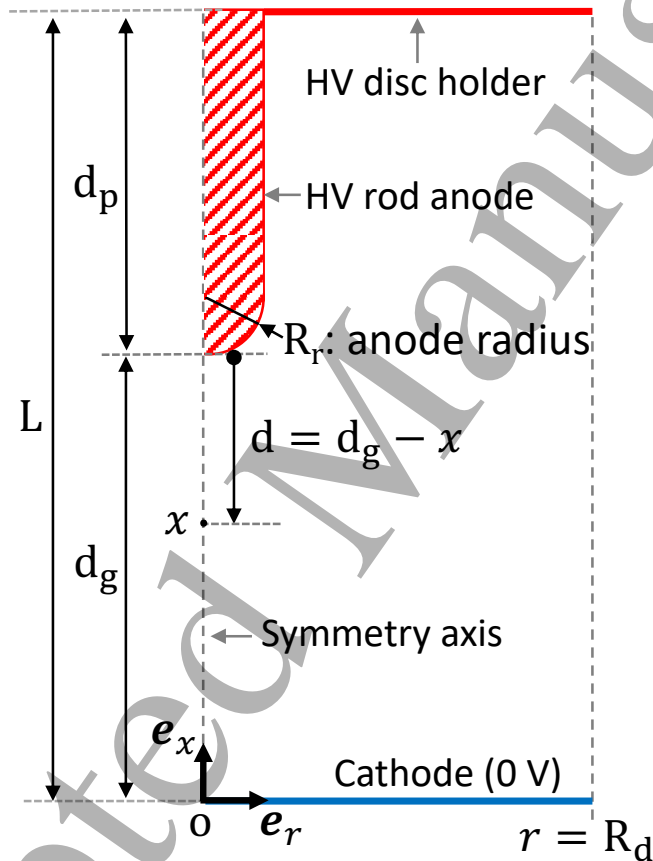


Figure 1. point-to-plane geometry with the rod electrode configuration.

hyperboloid electrode with a radius of curvature at its tip of 100 μm is used. Finally, in section 3.1.4, the radius R_d of the computational domain is varied between 1.6 and 7.5 cm. In all the simulations, the radius of the grounded cathode plane (and of the disc holder when it is present) is R_d .

In section 3.2, a time-varying applied voltage is used with a 1 ns rise time and a voltage plateau of 100 kV. As a base case, the high voltage electrode is a rod electrode ended with a semi-sphere of radius $R_r = 50 \mu\text{m}$. The computational domain is $L = 2.2 \text{ cm} \times R_d = 8.02 \text{ cm}$ with a Cartesian grid. In the axial direction, close to tip of

Morphology of positive ionization waves ...

6

the pin electrode (from $x = 1.3$ to 1.75 cm) a mesh size of $1 \mu\text{m}$ is used and then the mesh size is increased following a geometric progression up to $5 \mu\text{m}$ and is kept constant in the gas gap down to the cathode plane. From $x = 1.75$ cm to the upper boundary of the domain, the mesh size is increased from $1 \mu\text{m}$ up to $30 \mu\text{m}$ following a geometric progression and kept constant up to $x = 2.2$ cm. In the radial direction, a mesh size of $1 \mu\text{m}$ is used from the axis of symmetry up to $r = 0.07$ cm and is then increased to $5 \mu\text{m}$ and is kept constant up to $r = 1.257$ cm and then the mesh follows a geometric progression up to $30 \mu\text{m}$ and kept constant until $R_d = 8.02$ cm. Finally the grid used in this work is $n_x \times n_r = 7261 \times 3400$. In Section 3.2.1, a disc is set as holder of the rod electrode at $d_p = 0.6$ cm from its tip.

As in Bourdon et al. (2020), in this work, we have taken into account simplified boundary conditions for continuity equations at the anode and cathode surfaces. On the cathode plane, Neumann boundary conditions are applied for all charged particle fluxes. At the point anode and disc holder, the fluxes directed outward the electrode are estimated using Neumann boundary conditions for electrons and set to zero for ions. For Poisson's equation, at the metallic point anode-air interfaces, the ghost-fluid method is used (Celestin et al., 2009) with a Dirichlet boundary condition. The plane cathode in front of the point electrode is grounded (Figure 1). For the radial boundaries at $r = 0$ cm and $r = R_d$, Neumann boundary conditions are used. Other characteristics of the simulations (numerical methods and time-step calculation, code parallelization) are presented in detail in Pechereau (2013). As initial condition, a low uniform density of 10^4 cm^{-3} electrons and positive ions in air is considered, to be close to single pulse experiments in atmospheric pressure air at 300 K. In this work, we focus on the dynamics of the positive discharge propagation between the high voltage point anode electrode and the grounded cathode plane. Then, each simulation is stopped just after the connection of the discharge to the grounded cathode plane.

3. Results and discussion

3.1. Study of the discharge dynamics in a point-to-plane geometry with a 1.6 cm gap and an applied DC voltage of 50 kV

3.1.1. Influence of the radius of curvature R_r of the high voltage rod electrode

First, we present results on the discharge dynamics for a rod electrode with a radius $R_r = 100 \mu\text{m}$ set at $d_g = 1.6$ cm from a grounded plane cathode. For a DC applied voltage of 50 kV, Figure 2 shows the cross-sectional views of the absolute value of the electric field and electron density at $t = 0.5, 1.5$ and 2.74 ns. Table 1 gives the values of the ignition time τ_i (defined as the time a peak of electric field (corresponding to an ionization front) appears close to the high voltage pin electrode and starts propagating axially), the connection time τ_c (defined as the time the discharge connects to the grounded cathode plane) and the radius of the discharge at two locations in the inter-electrode gap at τ_c . With a DC voltage of 50 kV, the Laplacian electric field at the tip of

Morphology of positive ionization waves ...

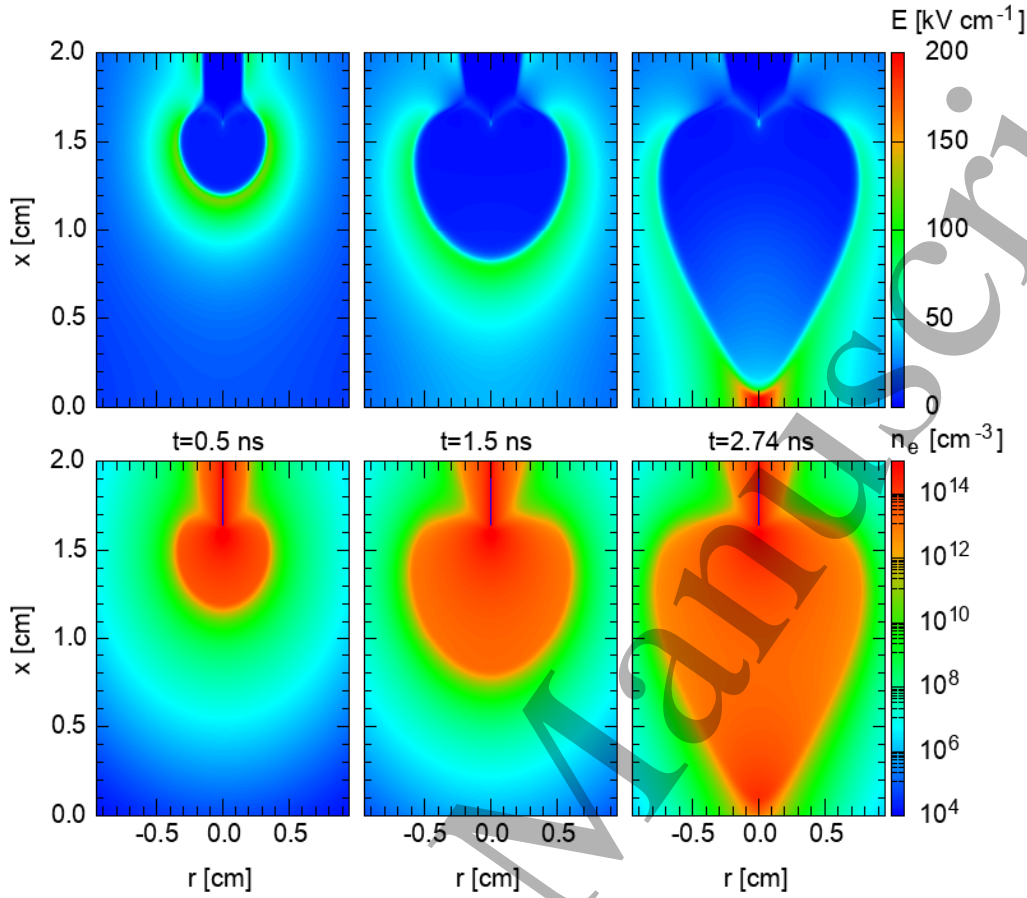


Figure 2. For a DC voltage of 50 kV and a high voltage rod electrode of radius $R_r = 100 \mu\text{m}$, cross-sectional views of the absolute value of the electric field and electron density at $t = 0.5, 1.5$ and $\tau_c = 2.74$ ns.

Table 1. Characteristics of the discharges obtained for rod electrodes with a radius R_r varying between 100 and 1000 μm .

Radius R_r of the rod electrode [μm]	100	200	500	1000
Ignition time τ_i [ns]	0.015	0.015	0.02	0.05
Connection time τ_c [ns]	2.74	2.77	2.82	3.06
Discharge radius at τ_c [cm]				
At $d = 2$ mm	0.79	0.80	0.82	0.86
At $d = 8$ mm	0.66	0.66	0.67	0.68

the rod electrode is of 3.2 MV cm^{-1} and then the ignition time τ_i is of only 0.015 ns. At $t = 0.5$ ns, Figure 2 shows that the discharge forms a sphere around the tip of the high

Morphology of positive ionization waves ...

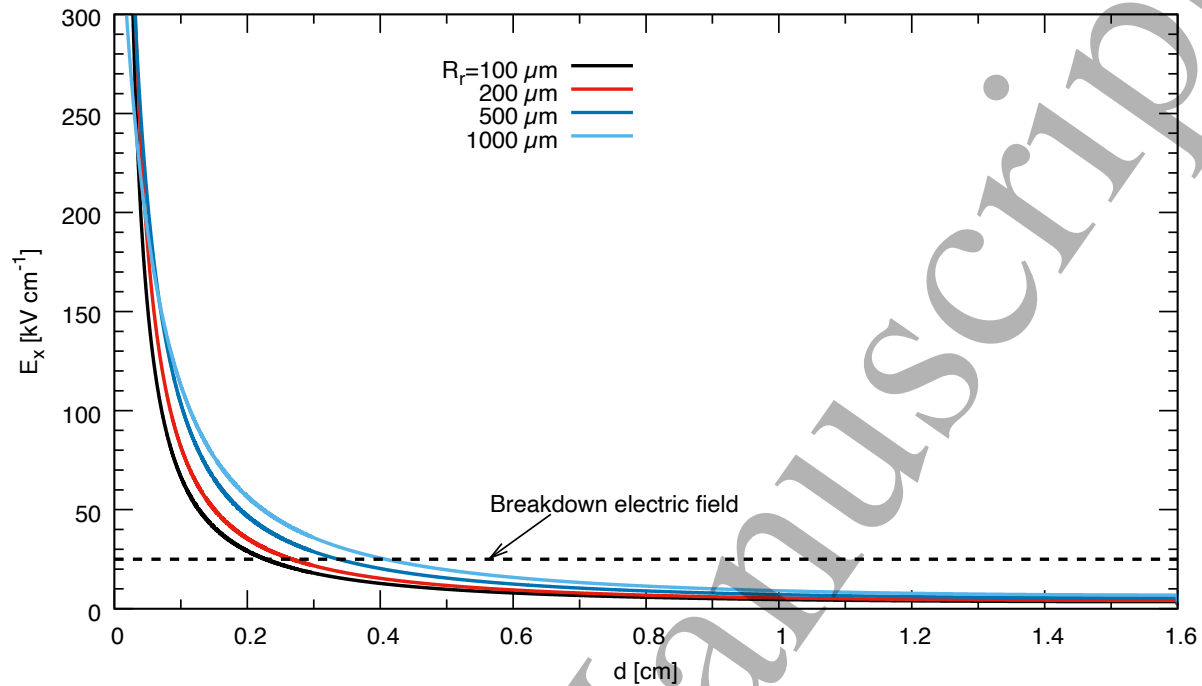


Figure 3. For a DC voltage of 50 kV and a high voltage rod electrode of radius $R_r = 100, 200, 500$ and $1000 \mu\text{m}$, Laplacian electric field on the symmetry axis as a function of the distance d from the anode tip.

voltage electrode. During the axial propagation of the discharge, its maximum radius increases until the discharge connects to the grounded cathode plane at $\tau_c = 2.74$ ns. At $t = \tau_c$, the discharge has a conical shape as observed in experiments (Tardiveau et al., 2009, 2016; Chng et al., 2019; Brisset et al., 2019) and simulations (Pechereau et al., 2014; Bourdon et al., 2020; Naidis et al., 2018; Zhu et al., 2021). The maximum radius of the discharge at $t = \tau_c$ is 0.79 cm at $d = 2$ mm from the tip. As observed already in Bourdon et al. (2020) without disc holder, a weak uniform radial discharge front propagates radially around the cylindrical part of the rod electrode and has a radius of 0.3 cm at τ_c .

Then, we study the influence of the radius R_r of the rod electrode, varying it between 100 and $1000 \mu\text{m}$, on the discharge dynamics and characteristics. As already mentioned in section 2, changing the radius of the rod electrode means changing both the radius of the rod and the radius of the semi-sphere at the tip, such that they always equal each other. With a DC applied voltage of 50 kV, the Laplacian electric field at the anode tip decreases from 3.2 MV cm^{-1} for $R_r = 100 \mu\text{m}$ to 410 kV cm^{-1} for $R_r = 1000 \mu\text{m}$. Figure 3 shows the evolution of the Laplacian electric field on the symmetry axis of the discharge. As expected, as the value of R_r increases from 100 to $1000 \mu\text{m}$, the region around the pin electrode where the electric field is higher than the breakdown field increases slightly. Figure 3 shows that the Laplacian electric field on the symmetry axis

Morphology of positive ionization waves ...

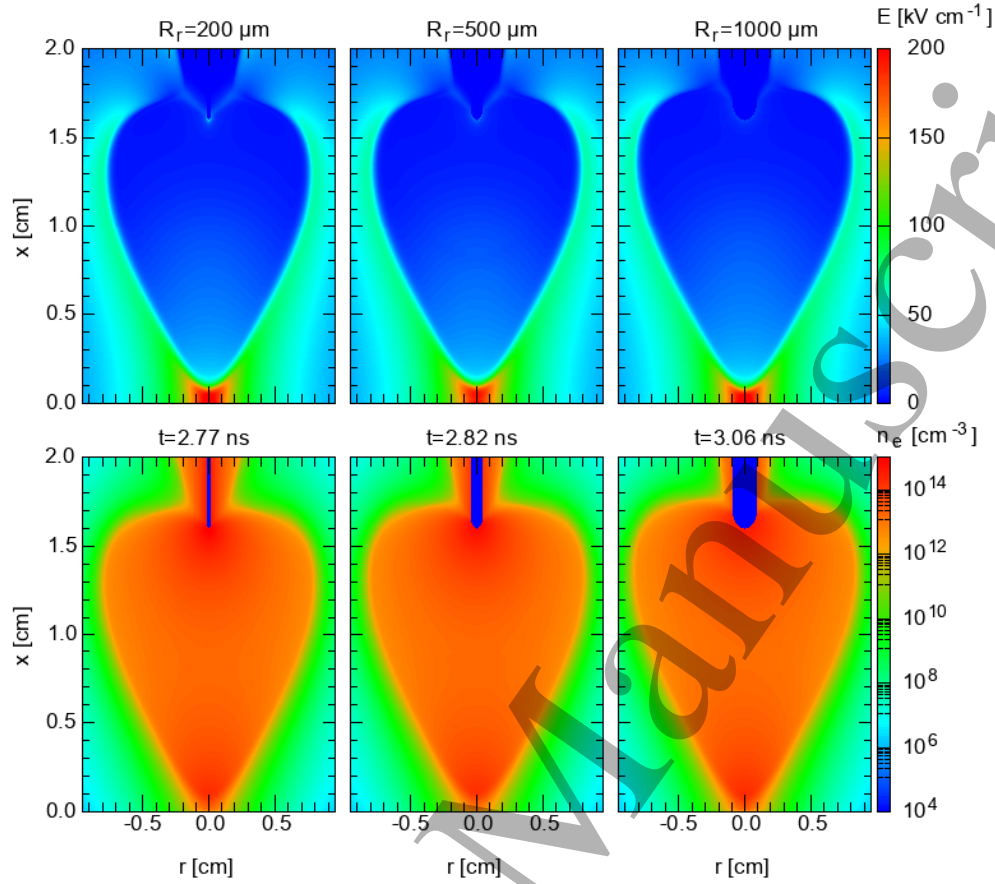


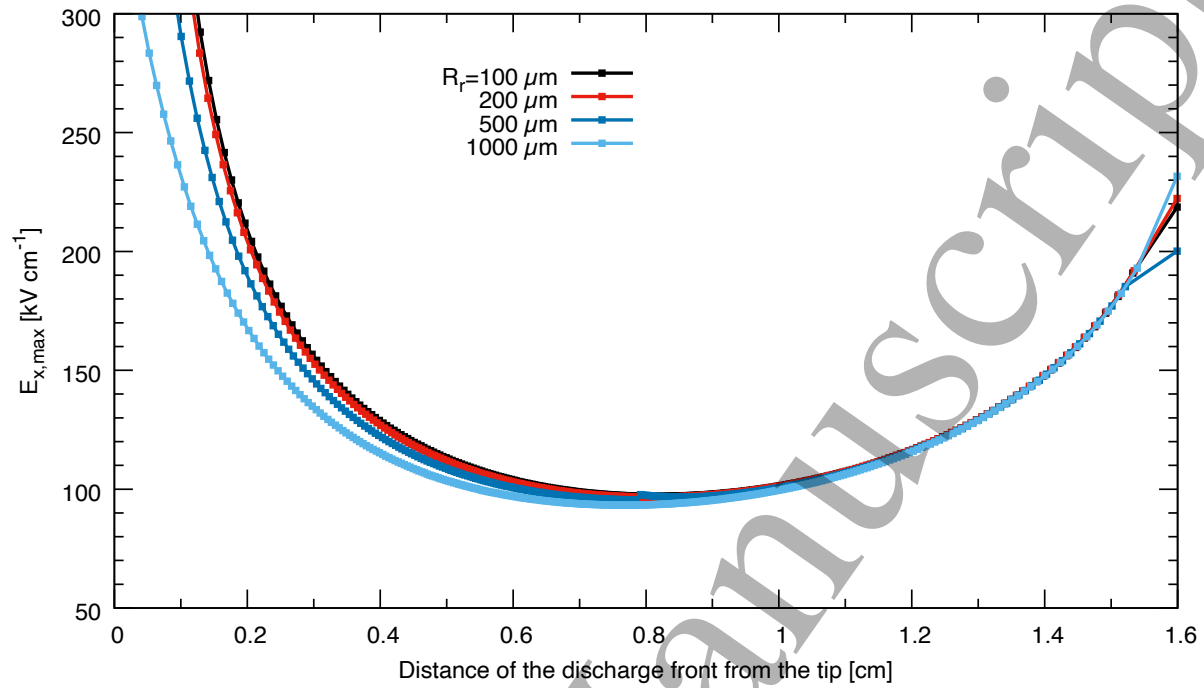
Figure 4. For a DC voltage of 50 kV and a high voltage rod electrode of radius $R_r = 200, 500$ and $1000 \mu\text{m}$, cross-sectional views of the absolute value of the electric field and electron density at the connection time at the cathode τ_c , i.e. at $t = 2.77, 2.82$ and 3.06 ns, respectively.

is below the breakdown field in most of the gap. In all cases, the ignition occurs close to the anode electrode with very short ignition times given in table 1. It is interesting to note that the connection time τ_c increases by a factor of 1.1 from 2.74 to 3.06 ns as the radius of the rod R_r increases by a factor 10 from 100 to 1000 μm . Figure 4 shows the cross-sectional views of the absolute value of the electric field and electron density at the connection times τ_c for rod electrodes with $R_r = 200, 500$ and $1000 \mu\text{m}$. In all the studied cases for R_r varying between 100 and 1000 μm , Figures 2 and 4 and Table 1 show that the discharge has a conical shape when it connects to the grounded cathode plane with a maximum radius that increases only slightly from 0.79 cm to 0.86 cm as R_r increases from 100 to 1000 μm .

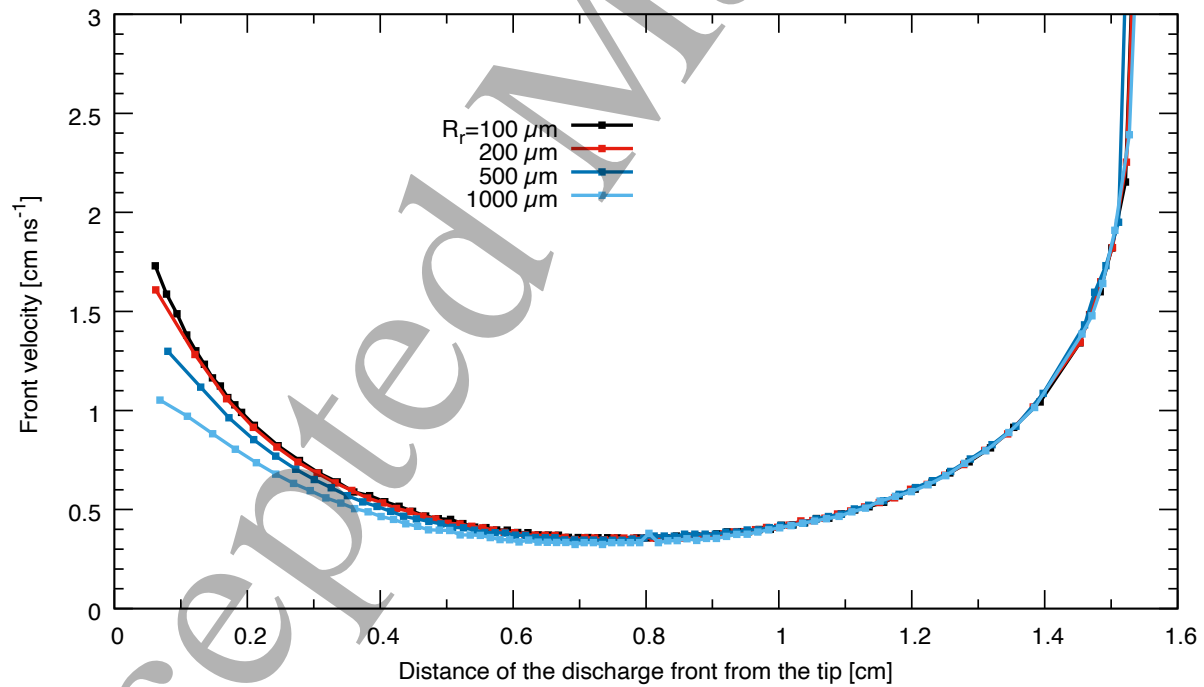
Then, this parametric numerical study confirms that a sharp high voltage point electrode is not mandatory to observe diffuse nanosecond positive ionization waves in point-to-

plane geometry. Indeed, in Babaeva and Naidis (2016b); Babaeva and Naidis (2016a) a spherical high voltage electrode of radius 0.5 and 0.25 cm, respectively, were used to simulate a positive diffuse discharge. Furthermore, in the simulations presented in Tarasenko et al. (2020), the sphere radius is varied between 0.1 and 0.15 cm for a constant DC applied voltage. It is shown that the influence of the tip radius on the average propagation velocity of the diffuse ionization wave is negligible, in agreement to the small variations of connection times τ_c presented in Table 1. The small influence of the radius of curvature of the high voltage point electrode on the discharge characteristics is also reported in the simulations carried out in Zhu et al. (2021) (radius of curvature of the tip varied between 50 to 100 μm) and in the experiments in Tardiveau et al. (2016) (radius of curvature of the tip varied between 10 to 200 μm). It is interesting to note that, in point-to-plane discharge simulations, the use of a blunt electrode allows to reduce numerical constraints on the mesh and time-step. Conversely, in experiments, sharp anode electrodes may be preferred to avoid parasite discharges or jitters at high voltages.

Figure 5 (a) shows the evolution of $E_{x,\text{max}}$, the maximum absolute value of the electric field in the discharge front on the symmetry axis of the discharge as a function of the distance of the discharge front from the tip, for a rod radius R_r varying between 100 and 1000 μm . The position of the discharge front is defined in this study as the distance between the location of the maximum absolute value of the field on the symmetry axis and the tip of the anode electrode. For all values of R_r , we observe that after ignition, the electric field in the discharge front decreases rapidly from 300 kV cm^{-1} for distances $d \leq 1 - 2$ mm from the tip to a minimal value varying from 97 to 93 kV cm^{-1} for $R_r = 100$ and 1000 μm , respectively. Then, as the discharge approaches the cathode plane, the value $E_{x,\text{max}}$ increases again. Based on the knowledge of the axial position of the discharge front in time, the axial propagation velocity of the discharge front is calculated as a function of the axial position of the discharge front and shown in Figure 5 (b) for R_r varying between 100 and 1000 μm . The velocity of the discharge front is calculated for distances from the tip $d \geq 0.5$ mm. We observe that for all values of R_r , the discharge front velocity first decreases from values in the range 1 to 1.8 cm ns^{-1} to a minimal value of about 0.4 cm ns^{-1} for $6 < d < 8$ mm, and then increases again as the discharge approaches the cathode plane. These values of discharge front velocities and maximum absolute value of the electric field in the discharge front are in good agreement with experimental and numerical results obtained for discharges in atmospheric pressure air in point-to-plane geometries with gaps of about 1 cm generated by high voltages applied with sub-nanosecond and nanosecond rise times, as reviewed in Naidis et al. (2018); Bourdon et al. (2020); Babaeva and Naidis (2021). Similar values of discharge front velocities have been also observed in sub-nanosecond pulsed discharges generated in a 1.2 mm pin-to-pin gap in air at atmospheric pressure (Höft et al., 2020). It is interesting to point out that the evolution of the front propagation velocity during its propagation shown in Figure 5 (b) is in agreement with the experimental and numerical results presented in Tarasenko et al. (2020) for a point-to-plane geometry with a 8.5 mm gap in atmospheric



(a)



(b)

Figure 5. For 50 kV DC discharges with rod electrodes of different radii R_r in the range 100–1000 μm , evolution of (a) the maximum absolute value of the axial electric field on the symmetry axis (b) the axial propagation velocity of the discharge front as a function of the distance of the discharge front from the anode tip.

pressure air. When the discharge front approaches the cathode, the discharge front velocity shown in Figure 5 (b) increases to values higher than 2 cm ns^{-1} . However, due to the interaction with the cathode, which is simplified in this work, the meaning of the discharge propagation velocity when the front approaches close to the cathode becomes open to discussion. Then in this work, we limit our analysis of the discharge propagation velocity to values less than an upper limit of about 3 cm ns^{-1} close to the cathode.

It is interesting to note that even if the radius R_r of the rod electrode is varied by a factor 10, the discharge dynamics and characteristics remain very close. The main differences are observed only for distances d less than 6 mm from the tip. The highest velocity close to the point anode electrode is obtained for the smallest tip radius, in agreement with the simulations presented in Tarasenko et al. (2020).

3.1.2. Influence of the presence and position of a disc as holder of the point anode electrode In this section, we model the presence of a holder for the point anode electrode as a simple metallic disc at 50 kV set at different distances d_p from the tip of the point anode electrode. In this work, the radius of the disc holder is the same as the computational domain ($R_d = 7.5 \text{ cm}$) to avoid any radial discharge propagation from the edges of the high voltage disc. First, it is important to note that adding a high-voltage disc has a major impact of the Laplacian electric field. With a DC high voltage of 50 kV, for a rod electrode of $R_r = 100 \mu\text{m}$ without disc, the Laplacian electric field at the tip of the anode is of 3.2 MV cm^{-1} . With a disc holder, the Laplacian electric field at the tip decreases as the distance d_p of the disc to the tip decreases and is for example of 2.27 MV cm^{-1} for $d_p = 4.8 \text{ cm}$ and only of 1.47 MV cm^{-1} for $d_p = 1 \text{ cm}$. Figure 6 shows the axial evolution of the Laplacian electric field on the symmetry axis without disc holder and for a disc holder set at $d_p = 0.6, 1, 1.6$ and 4.8 cm . It is interesting to note that as d_p decreases, the Laplacian electric field on the symmetry axis decreases close to the tip of the anode for $d < 2 \text{ mm}$ but increases in the gap for $d > 2 \text{ mm}$ and becomes close to the breakdown electric field. At the border of the computational domain ($r = R_d = 7.5 \text{ cm}$, far from the sharp rod), with a disc holder, the Laplacian electric field has only a constant axial component, which value depends on the disc holder position and varies between 7.9 to 22.7 kV cm^{-1} as d_p varies between 4.8 to 0.6 cm . Then, the presence and position of a disc holder distort significantly the Laplacian equipotential lines in the studied point-to-plane geometry.

Figures 2, 7 and Table 2 show the discharge dynamics and characteristics for a rod electrode of $R_r = 100 \mu\text{m}$ with a disc holder set at $d_p = 0.6, 1, 1.6$ and 4.8 cm and without a disc holder. In Table 2, we note that the location of the disc holder has a very small influence on the ignition time which remains very small for all studied cases. Conversely, the location of the disc holder has a major influence on the connection time which decreases from 4.14 ns to 2.92 ns as the disc holder moves from $d_p = 0.6 \text{ cm}$ to 4.8 cm . It is interesting to note that the connection time for a disc holder set at $d_p = 4.8 \text{ cm}$ from the anode tip is still 0.18 ns longer than the reference connection

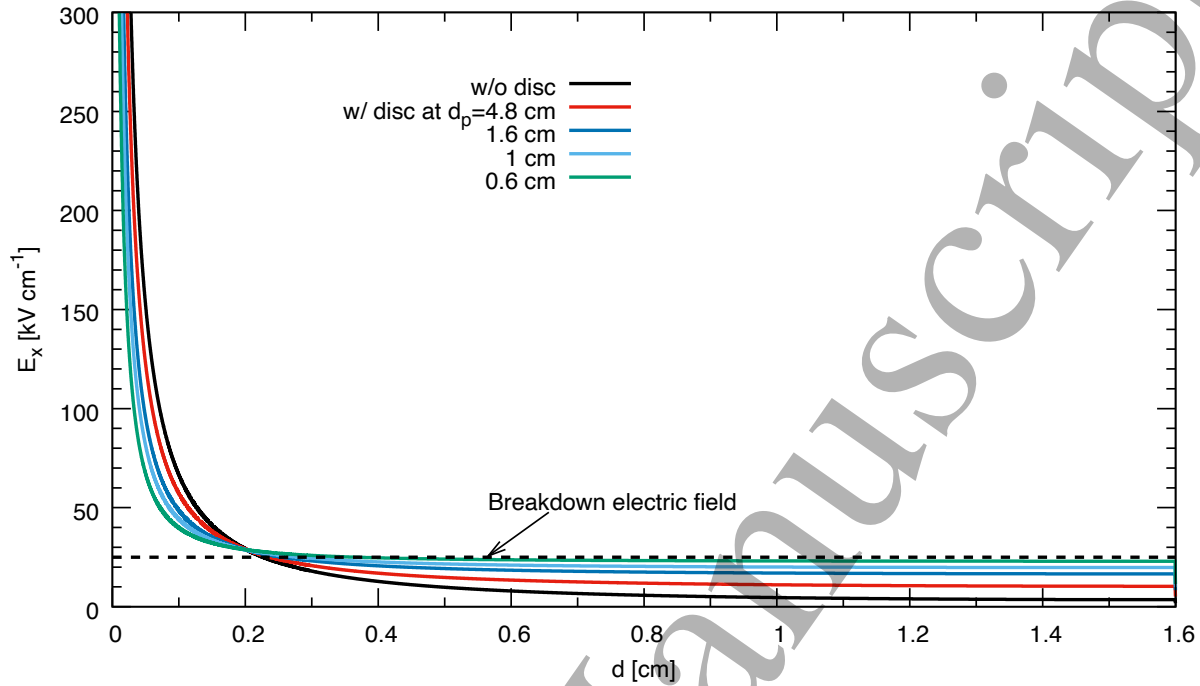


Figure 6. For a DC voltage of 50 kV and a high voltage rod electrode of $R_r = 100 \mu\text{m}$, axial evolution of the Laplacian electric field on the symmetry axis without a disc holder and with a disc holder at $d_p = 0.6, 1, 1.6$ and 4.8 cm.

time without disc. Figure 7 shows the cross-sectional views of the absolute value of the electric field and electron density at the connection times for disc holders set at $d_p = 0.6, 1.6$ and 4.8 cm from the anode tip. We note that the location of a disc holder has a major impact on the discharge morphology at the connection time. The shape of the discharge is conical without disc holder as observed on Figure 2 and as a disc holder is moved closer to the tip, the maximum radius decreases and moves farther from the tip and then the discharge shape becomes an ellipsoid. In particular, in Table 2, we note that the maximum discharge radius for $d_p = 4.8$ cm is 0.59 cm and is at $d = 2$ mm from the tip. For $d_p = 0.6$ cm, the maximum discharge radius is 0.24 cm and is at $d = 8$ mm from the tip. Finally, we note that the closer is the disc holder to the anode tip, the slower and weaker is the radial discharge around the cylindrical part of the rod electrode.

Figure 8 (a) shows the evolution of $E_{x,\text{max}}$, the maximal absolute value of the electric field on the symmetry axis of the discharge as a function of the axial position of the discharge front for a disc holder set at $d_p = 0.6, 1, 1.6$ and 4.8 cm with a case without disc holder. For all cases, we observe that rapidly after ignition, the electric field in the discharge front decreases rapidly as the discharge starts propagating axially. In all studied conditions, $E_{x,\text{max}}$ remains less than 150 kV cm^{-1} over most of the gap distance. Only when the discharge front approaches close to the grounded cathode plane, $E_{x,\text{max}}$

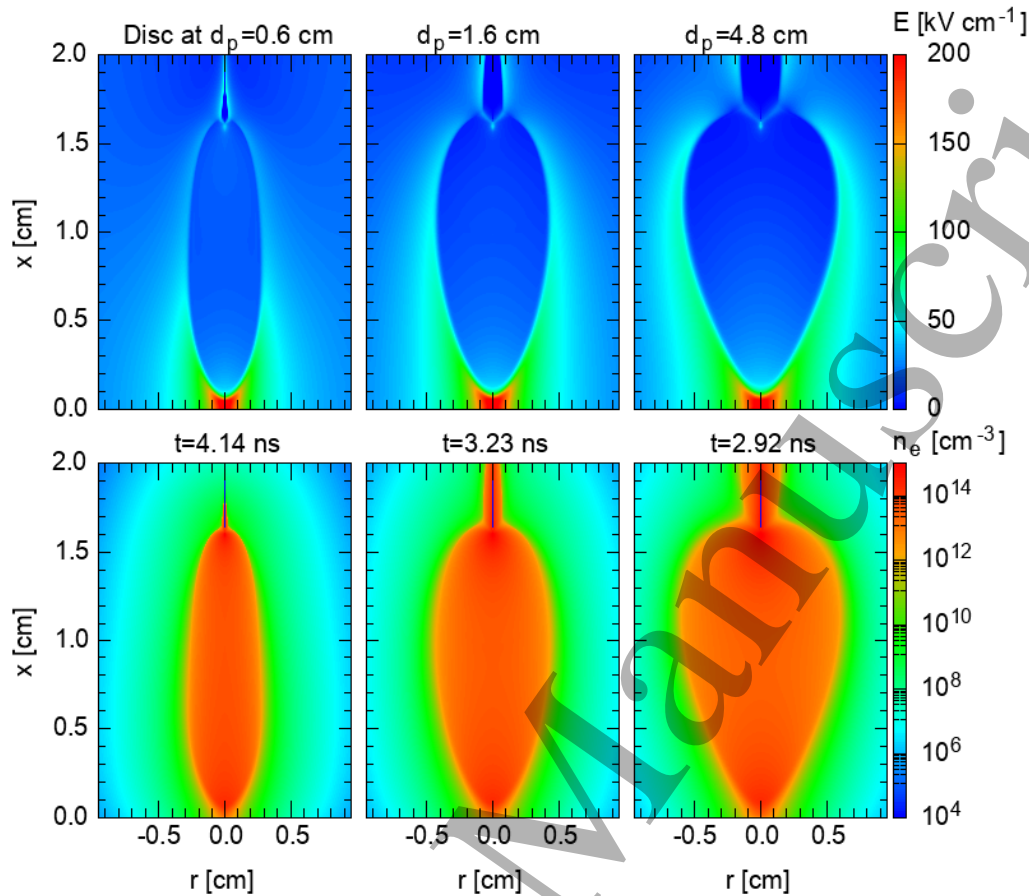
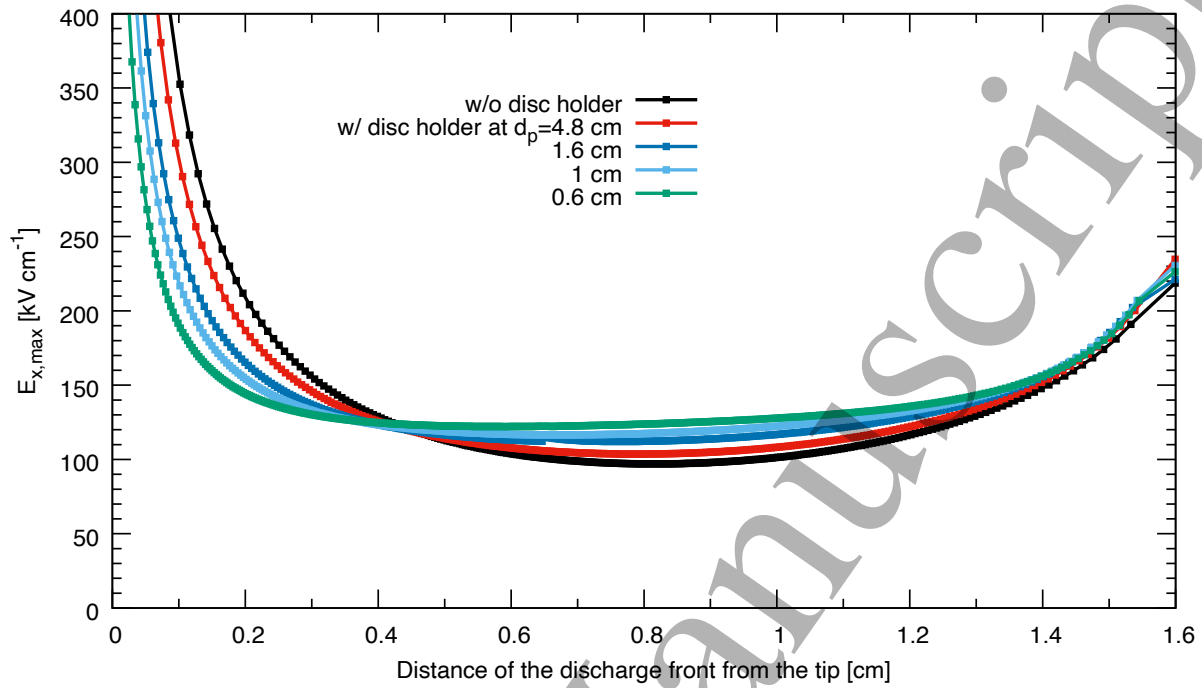
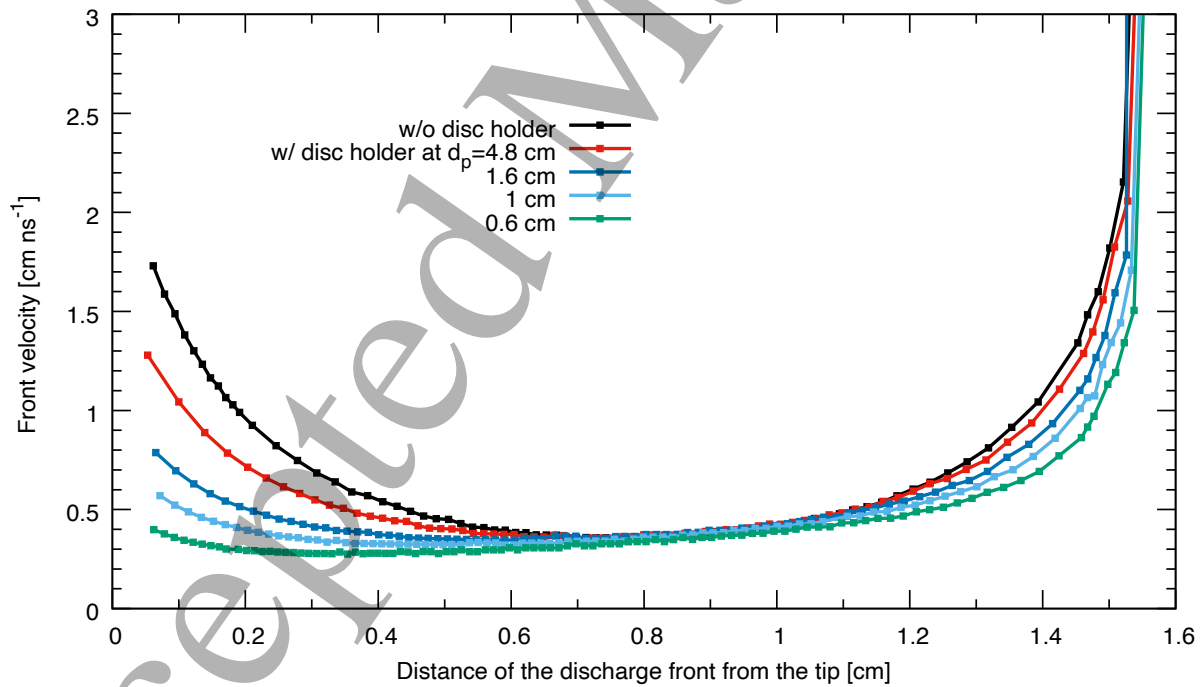


Figure 7. For a DC voltage of 50 kV and a high voltage rod electrode of $R_r = 100 \mu\text{m}$ with a disc holder at $d_p = 0.6, 1.6$ and 4.8 cm of the tip, cross-sectional views of the absolute value of the electric field and electron density at the connection time at the cathode τ_c , i.e. at $t = 4.14, 3.23$ and 2.92 ns, respectively.

increases again. Figure 8 (b) shows the velocity of the discharge front for the same conditions. The velocity of the discharge front is calculated for $d > 0.5$ mm. For all studied conditions, the discharge front velocity first decreases from values in the range 0.4 to 1.8 cm ns^{-1} to a minimal value varying between 0.3 to 0.4 cm ns^{-1} and then increases again, reaching values higher than 2 cm ns^{-1} as the discharge approaches the plane cathode electrode. Close to the point anode electrode, it is interesting to note the highest propagation velocity is obtained without a disc holder and decreases as the disc holder is set closer to the tip of the point anode electrode. In fact, without a disc holder, the discharge front starts developing as a sphere which appears to give the fastest propagation. With a disc holder, we observe that due to the changes of the Laplacian equipotential lines, the radial expansion of the discharge close to the point anode electrode is constrained, which gives a lower axial propagation velocity of the



(a)



(b)

Figure 8. For a DC voltage of 50 kV and as high voltage electrode, a high voltage rod electrode of $R_r = 100 \mu\text{m}$ with a disc holder at $d_p = 0.6, 1, 1.6$ and 4.8 cm of the tip and without disc holder, evolution of (a) $E_{x,\text{max}}$, the maximum absolute value of the electric field on the symmetry axis of the discharge, and (b) the velocity of the discharge front as a function of the distance of the discharge front from the anode tip.

Morphology of positive ionization waves ...

16

discharge front in the gap.

Table 2. Characteristics of the discharges obtained for a DC voltage of 50 kV and as high voltage electrode, a rod electrode with $R_r = 100 \mu\text{m}$ and a disc holder at $d_p = 0.6, 1, 1.6$ and 4.8 cm of the tip of the anode electrode and without disc holder ($d_p = \infty$).

Disc holder at d_p [cm]	∞	4.8	1.6	1	0.6
Ignition time τ_i [ns]	0.015	0.015	0.015	0.02	0.03
Connection time τ_c [ns]	2.74	2.92	3.23	3.61	4.14
Discharge radius at τ_c [cm]					
At $d=2$ mm	0.79	0.59	0.41	0.32	0.24
At $d=8$ mm	0.66	0.56	0.45	0.38	0.31

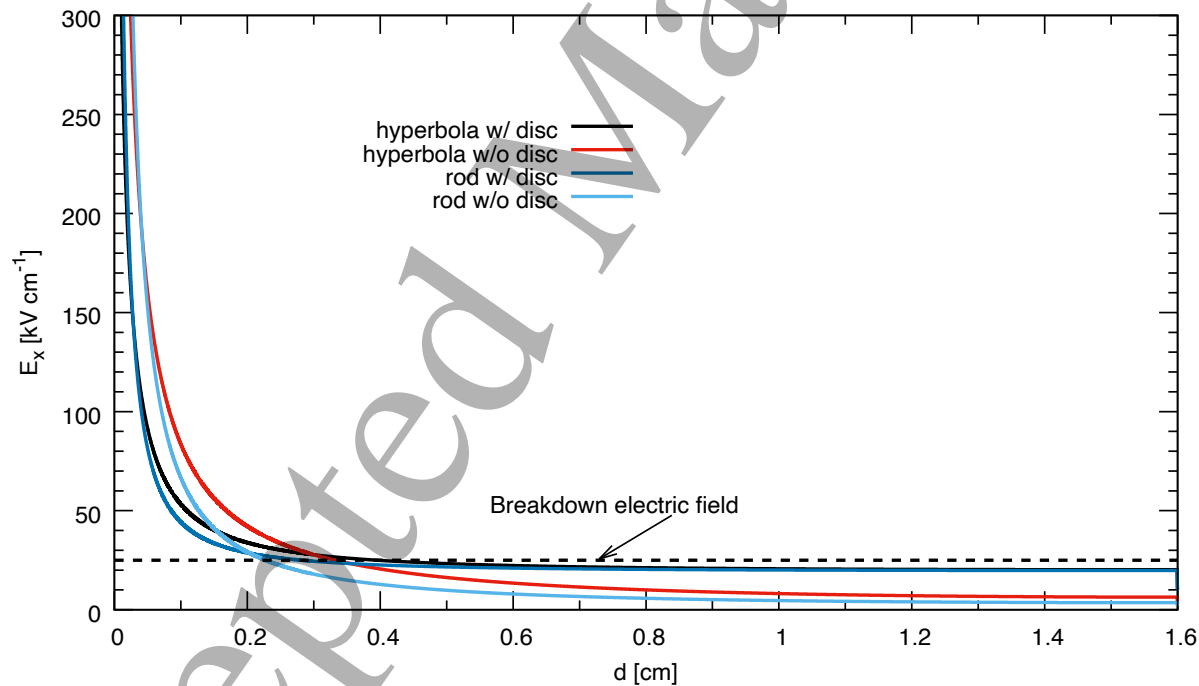


Figure 9. For a DC voltage of 50 kV, evolution of the Laplacian electric field on the symmetry axis for a rod electrode of $R_r = 100 \mu\text{m}$ without and with a disc holder at $d_p = 1$ cm and for a hyperbola with a radius of curvature of $100 \mu\text{m}$ without and with a disc holder at $d_p = 1$ cm.

3.1.3. Influence of the shape of the high voltage point anode electrode To study the influence of the shape of the high voltage point anode electrode, we compare results obtained for a hyperboloid high voltage anode electrode (defined by $(x/b)^2 - (r/a)^2 = 1$ with $b = 1.6$ cm and $a = 0.1265$ cm) with a radius of curvature of $a^2/b = 100 \mu\text{m}$ at

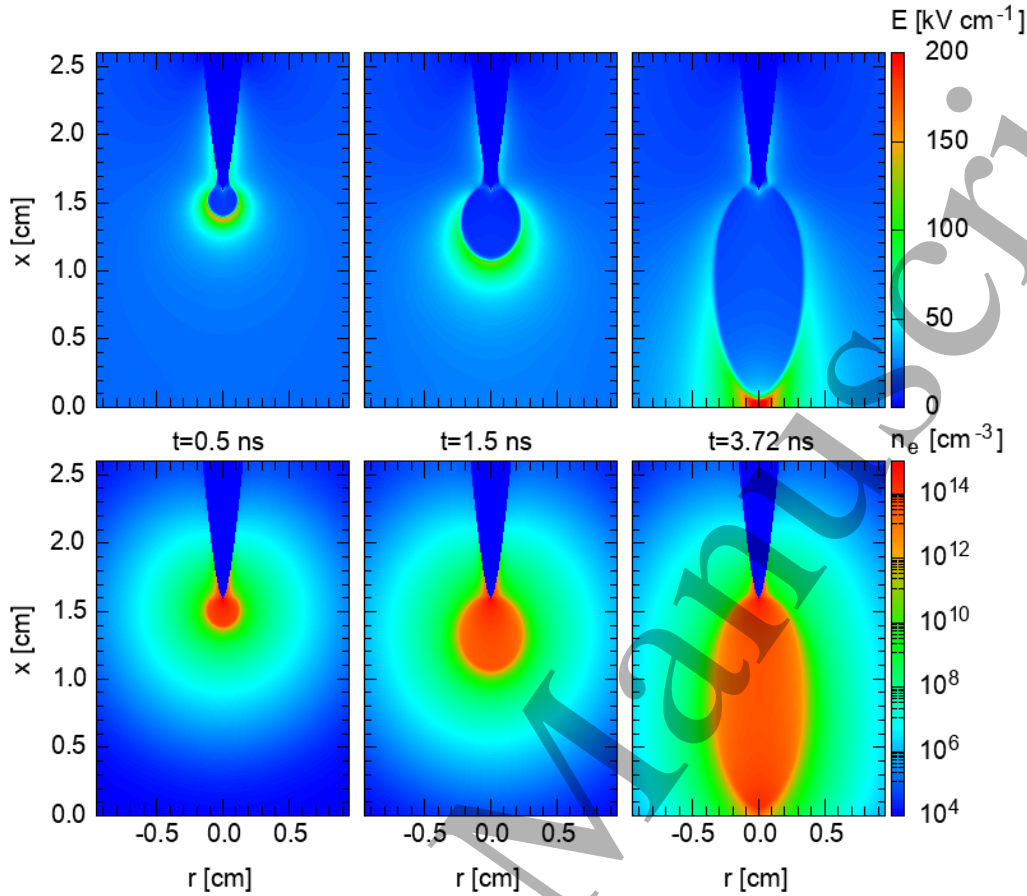


Figure 10. For a DC voltage of 50 kV and a hyperboloid point anode $((x/b)^2 - (r/a)^2 = 1$ with $b = 1.6 \text{ cm}$ and $a = 0.1265 \text{ cm}$) with a radius of curvature of $a^2/b = 100 \mu\text{m}$ at its tip with a disc holder at $d_p = 1 \text{ cm}$, cross-sectional views of the absolute value of the electric field and electron density at $t = 0.5, 1.5$ and 3.72 ns .

its tip with results obtained for a rod electrode with $R_r = 100 \mu\text{m}$. Figure 9 shows the axial evolution of the Laplacian electric field on the symmetry axis for both anode shapes, with and without a disc holder set at $d_p = 1 \text{ cm}$ of the anode tip. Without a disc holder, the peak electric field at the anode tip is 3.2 MV cm^{-1} for the rod electrode and decreases to 1.73 MV cm^{-1} for the hyperbola. However, in the gap, for $d > 1 \text{ mm}$, Figure 9 shows that the Laplacian electric field on the symmetry axis obtained for an hyperbola is slightly higher than for a rod. With a disc holder, the peak electric field at the rod tip decreases to 1.47 MV cm^{-1} and to 0.92 MV cm^{-1} for the hyperboloid electrode. In the gap, Figure 9 shows that, with a disc holder, for $d > 4 \text{ mm}$, the Laplacian electric field on the symmetry axis in the gap is very close for both anode shapes and is higher than without a disc holder.

For a DC applied voltage of 50kV, Figure 10 shows the cross-sectional views of the

Morphology of positive ionization waves ...

18

absolute value of the electric field and electron density at $t = 0.5, 1.5$ and 3.72 ns for the hyperboloid high voltage electrode with a radius of curvature of the tip of $100 \mu\text{m}$ with a disc holder set at $d_p = 1$ cm from the tip. The disc holder allows to avoid any parasite radial discharge initiated by the sharp edge of the hyperboloid electrode at the upper boundary of the computational domain. As the Laplacian electric field is much higher than the breakdown field close to the anode tip (Figure 9), the discharge ignition time is very short and at $t = 0.5$ ns, the discharge forms a sphere around the tip of the hyperboloid electrode. The radius of the discharge increases during the axial propagation of the discharge and reaches a maximum value of 0.38 cm in the middle of the gap, at the time of the connection to the grounded cathode at $t = \tau_c = 3.72$ ns. At connection, the discharge has an ellipsoid shape. For both rod and hyperboloid electrodes with a tip radius of $R_r = 100 \mu\text{m}$ with and without disc holder, Table 3 compares the values of ignition time τ_i and connection time τ_c to the grounded cathode plane and the radius of the discharge at two locations in the inter-electrode gap at τ_c . Figure 11 shows the cross-sectional views of the absolute value of the electric field and electron density at the connection times for a rod electrode with $R_r = 100 \mu\text{m}$ with a disc holder, a hyperboloid electrode with a radius of curvature at its tip of $100 \mu\text{m}$ with a disc holder shown in Figure 10; and for same hyperboloid electrode without disc holder. Figures 11 and 10 and Table 3 show that the shape of the point electrode (either a rod electrode or an hyperbola) has only a small influence on the ignition and connection times and discharge radius at the connection time. Conversely, as shown for the rod electrode in section 3.1.2, for a hyperboloid electrode, the presence or not of a disc holder has a significant impact on the discharge propagation in the gap, the maximum radius and the shape of the discharge at the connection time. As observed in section 3.1.2, with a disc holder, the maximum radius of the discharge at the connection time decreases and is located farther from the anode tip. Same trends have been observed in Zhu et al. (2021) and attributed to the change of the shape of the anode tip. However, the detailed parametric study presented in the present work allows to distinguish the role of the shape of the point anode and of its holder.

Figure 12 compares the maximum absolute value of the electric field on the symmetry axis and the axial propagation velocity of the discharge front as a function of the axial position of the discharge front for the 3 geometries shown in Figures 11 and 10. We clearly see that the shape of the high voltage point electrode (either rod or hyperbola) has an almost negligible influence on the discharge characteristics in comparison to the effect of the presence of a disc holder.

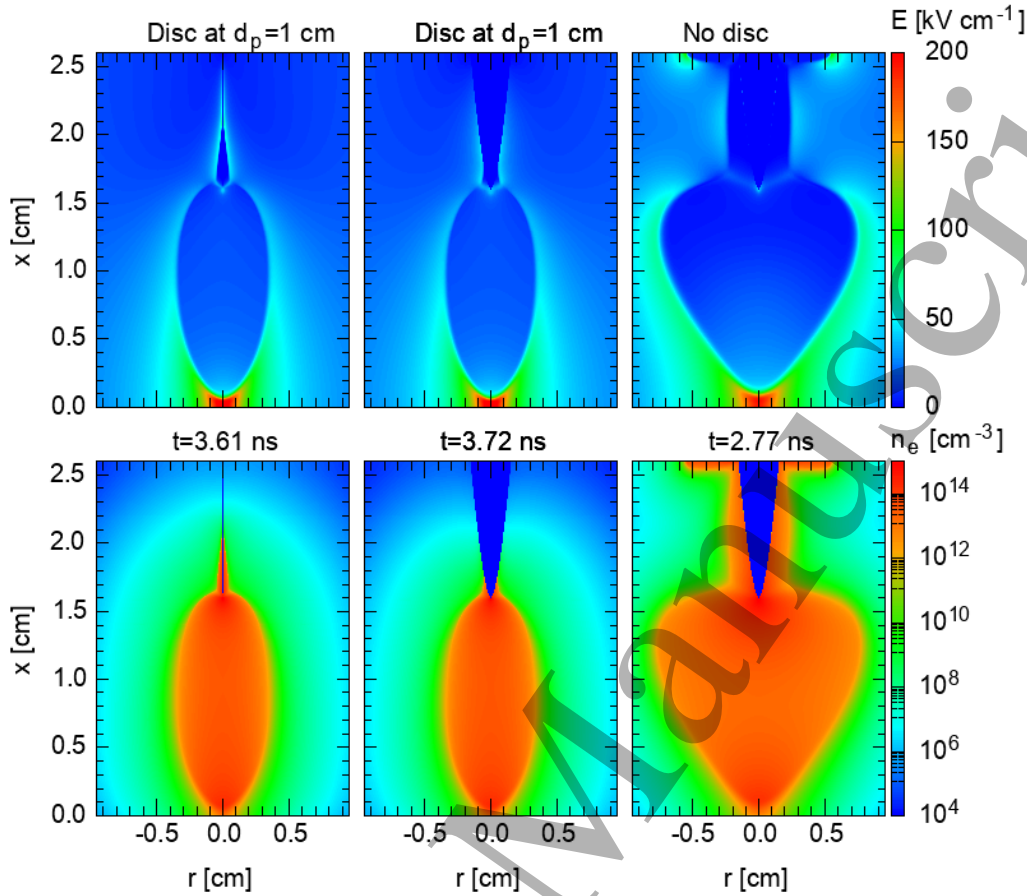
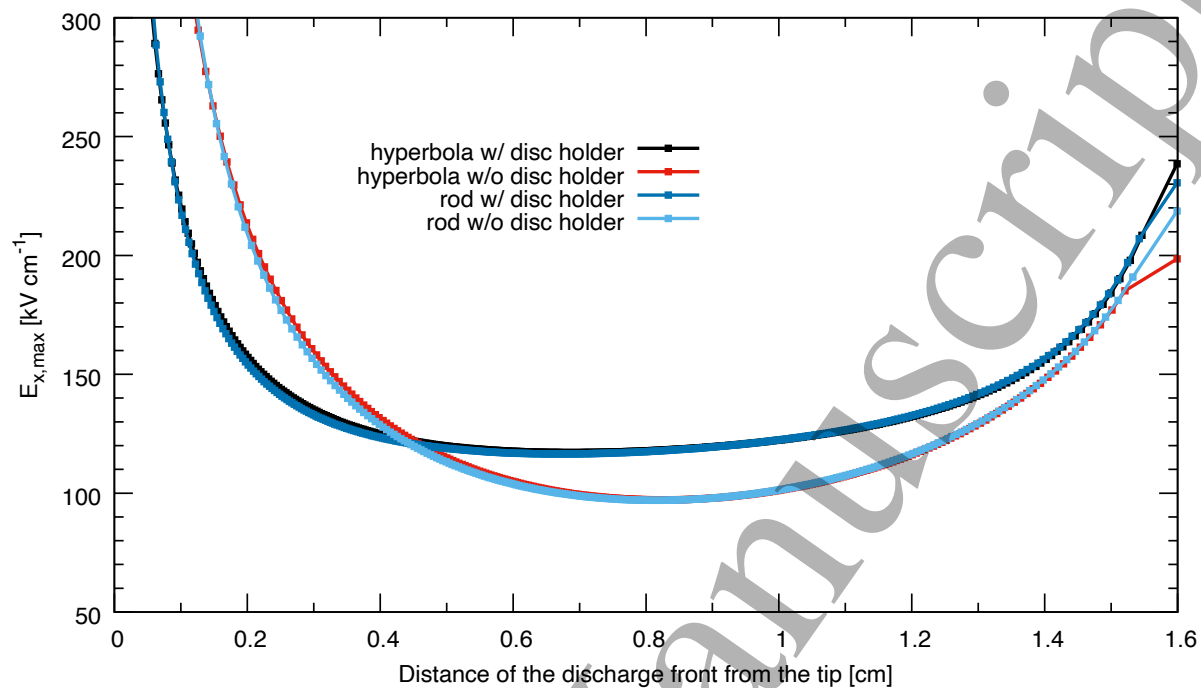
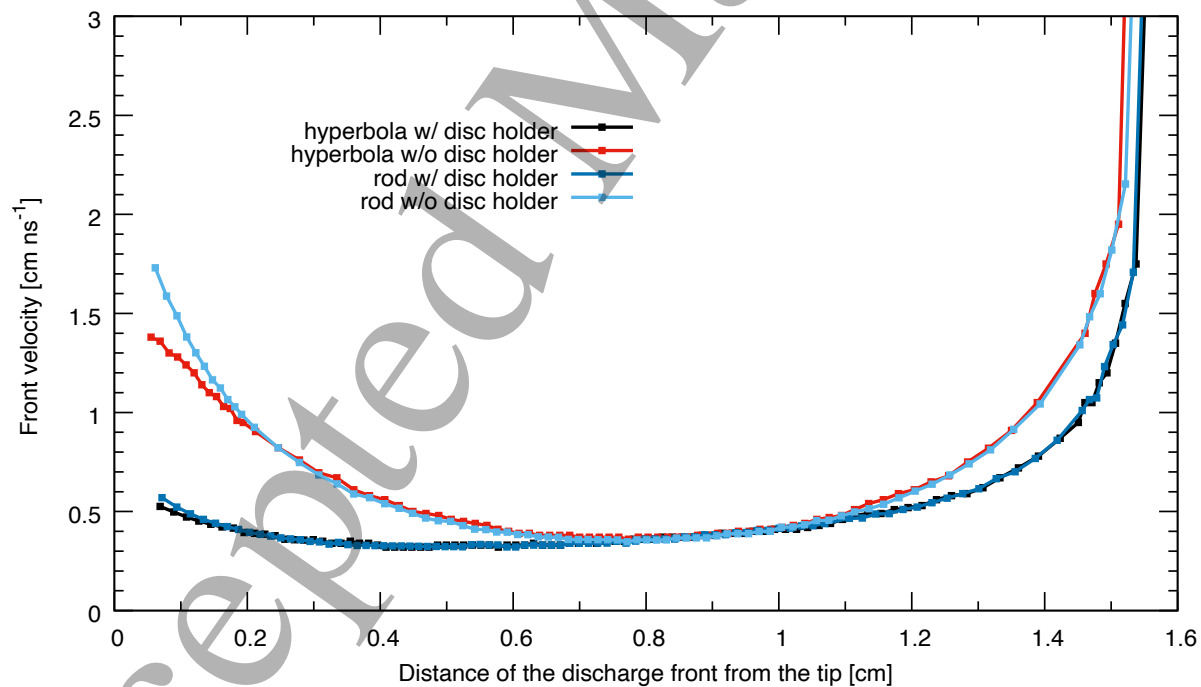


Figure 11. For a DC voltage of 50 kV and as high voltage electrode: a rod electrode with $R_r = 100 \mu\text{m}$ and a disc holder at $d_p = 1 \text{ cm}$; a hyperbola with a radius of curvature of $100 \mu\text{m}$ at its tip with a disc holder at $d_p = 1 \text{ cm}$; the same hyperbola without a disc holder, cross-sectional views of the absolute value of the electric field and electron density at the connection time at the cathode, i.e. at $t = 3.61$, 3.72 and 2.77 ns , respectively.

3.1.4. Influence of the radius of the computational domain R_d In this section, we consider the base case of section 3.1.1 with a rod electrode of $R_r = 100 \mu\text{m}$, without a disc holder and we vary the radius of the computational domain from the reference value of $R_d = 7.5 \text{ cm}$ to 1.6 cm . Figure 13 shows the cross-sectional views of the absolute value of the electric field and electron density at the connection times for $R_d = 5$, 3 and 1.6 cm . If we compare with Figure 2 for $R_d = 7.5 \text{ cm}$, we notice, that there is no influence of the value of R_d on the results for $R_d \geq 5 \text{ cm}$. Conversely, Figure 13 shows that for $R_d \leq 5 \text{ cm}$, at the connection time, the discharge shape changes from a conical shape for $R_d = 5 \text{ cm}$ to a more ellipsoidal shape with a smaller maximum radius for $R_d = 1.6 \text{ cm}$.



(a)



(b)

Figure 12. For a DC voltage of 50 kV and as high voltage electrode: a hyperbola with a radius of curvature of $100 \mu\text{m}$ at its tip with and without a disc holder at $d_p = 1 \text{ cm}$; a rod electrode with $R_r = 100 \mu\text{m}$ with and without a disc holder at $d_p = 1 \text{ cm}$, evolution of (a) $E_{x,\text{max}}$, the maximum absolute value of the electric field on the symmetry axis of the discharge (b) the velocity of the discharge front as a function of the distance of the discharge front from the anode tip.

Table 3. Characteristics of the discharges obtained for a DC voltage of 50 kV and as high voltage electrode: an hyperbola with a radius of curvature of 100 μm at its tip with and without a disc holder at $d_p = 1$ cm; a rod electrode with $R_r = 100$ μm with and without a disc holder at $d_p = 1$ cm.

DC 50 kV	Hyperbola	Rod	Rod	Hyperbola
Disc holder	w/	w/	w/o	w/o
Ignition time τ_i [ns]	0.035	0.025	0.015	0.075
Connection time τ_c [ns]	3.72	3.61	2.74	2.77
Discharge radius at τ_c [cm]				
At $d=2$ mm	0.3	0.32	0.79	0.77
At $d=8$ mm	0.38	0.38	0.66	0.66

Table 4 gives the values of ignition time τ_i and connection time τ_c to the grounded cathode plane and the radius of the discharge at two locations in the inter-electrode gap at τ_c for the same conditions as Figures 13 and 2. We note that the connection time remains the same for $R_d > 3$ cm and is equal to 2.74 ns and increases up to 2.96 ns for $R_d = 1.6$ cm. The maximum radius at $d = 2$ mm remains constant when R_d decreases from 7.5 to 5 cm and then decreases down to 0.48 cm for $R_d = 1.6$ cm.

Figure 14 compares the maximum absolute value of the electric field on the symmetry axis and the axial propagation velocity of the discharge front as a function of the axial distance from tip on the symmetry axis for $R_d = 1.6, 3, 5$ and 7.5 cm. We note that the value of R_d has an almost negligible influence on the evolution of $E_{x,\max}$ and on the propagation velocity of the discharge front for $R_d > 3$ cm $\simeq 2d_g$. Therefore, in diffuse discharge simulations with Neumann boundary conditions for Poisson's equation at R_d , it is necessary to use at least a radial domain which is larger than 2 times the gap distance d_g to study the diffuse discharge characteristics on the discharge axis and a radial domain which is at least 3 times the gap distance d_g to study the maximum radius of the diffuse discharge at the connection time. In the simulations carried out in Tardiveau et al. (2016); Marode et al. (2016); Brisset et al. (2019) a radial domain of $R_d = 1$ cm is used and a disc is set at 1 cm from the anode tip. Based on the results of section 3.1.2 and of this section, both the effects of the disc holder and the reduced radial computational domain could explain why the authors obtained a good agreement with experiments only at very early times (≤ 1 ns) and then observed that the simulated discharge propagation velocity was smaller than in experiments.

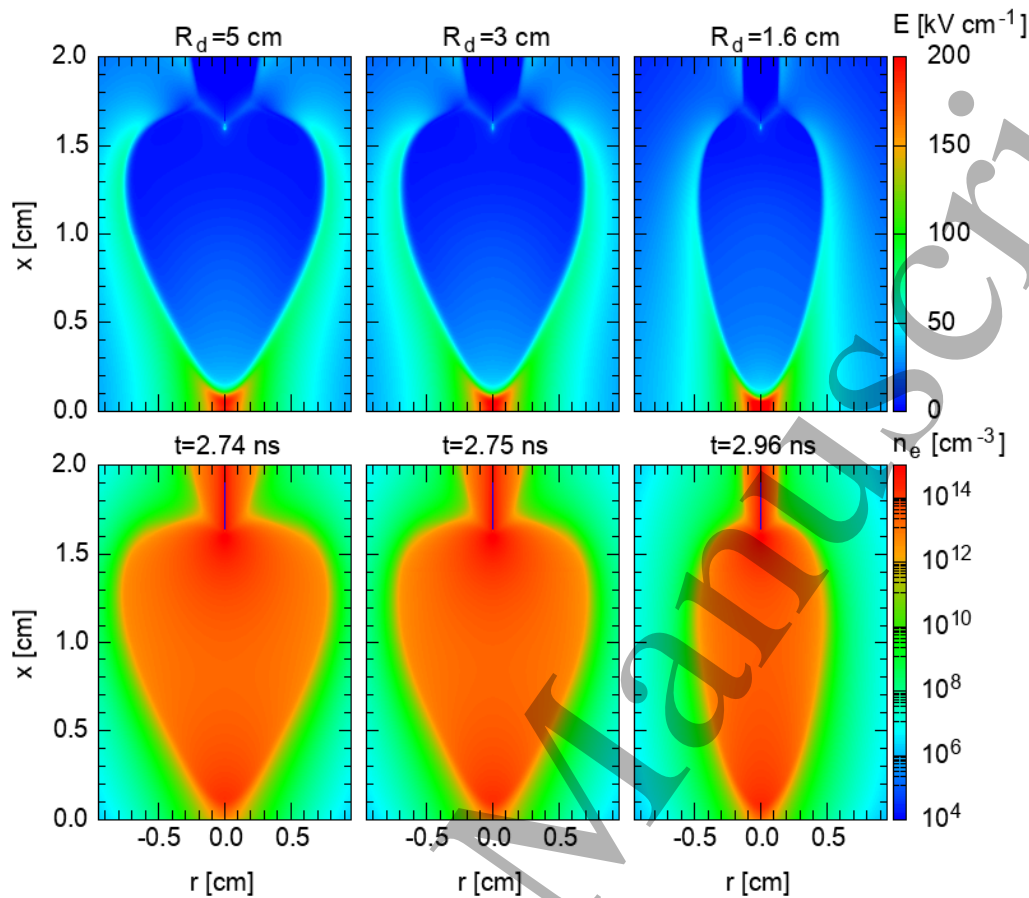


Figure 13. For a DC voltage of 50 kV and a high voltage rod electrode of $R_r = 100 \mu\text{m}$ without a disc holder and for different radius $R_d = 5, 3$ and 1.6 cm of the computational domain, cross-sectional views of the absolute value of the electric field and electron density at the connection time at the cathode, i.e. at $t = 2.74, 2.75$ and 2.96 ns, respectively

Table 4. Characteristics of the discharges obtained for a DC voltage of 50 kV and a high voltage rod electrode of $R_r = 100 \mu\text{m}$ without a disc holder and for a computational domain of radius $R_d = 7.5, 5, 3$ and 1.6 cm.

R_d [cm]	7.5	5	3	1.6
Ignition time τ_i [ns]	0.015	0.015	0.015	0.015
Connection time τ_c [ns]	2.74	2.74	2.75	2.96
Discharge radius at τ_c [cm]				
At $d = 2$ mm	0.79	0.79	0.72	0.48
At $d = 8$ mm	0.66	0.66	0.63	0.46

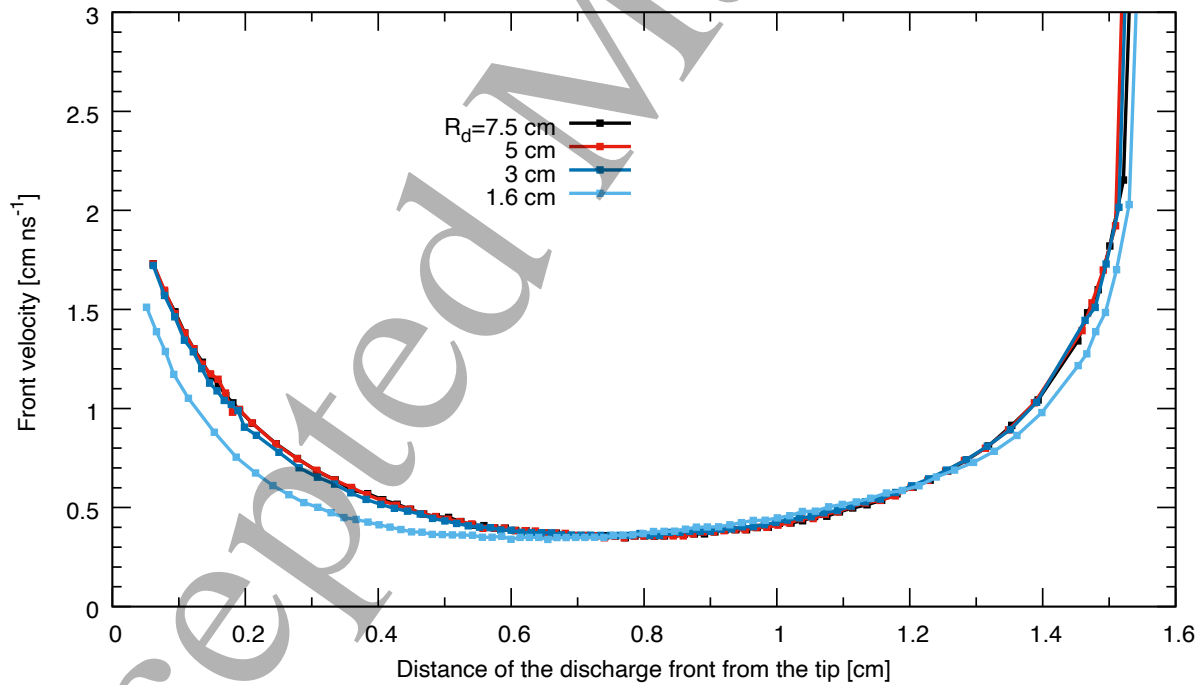
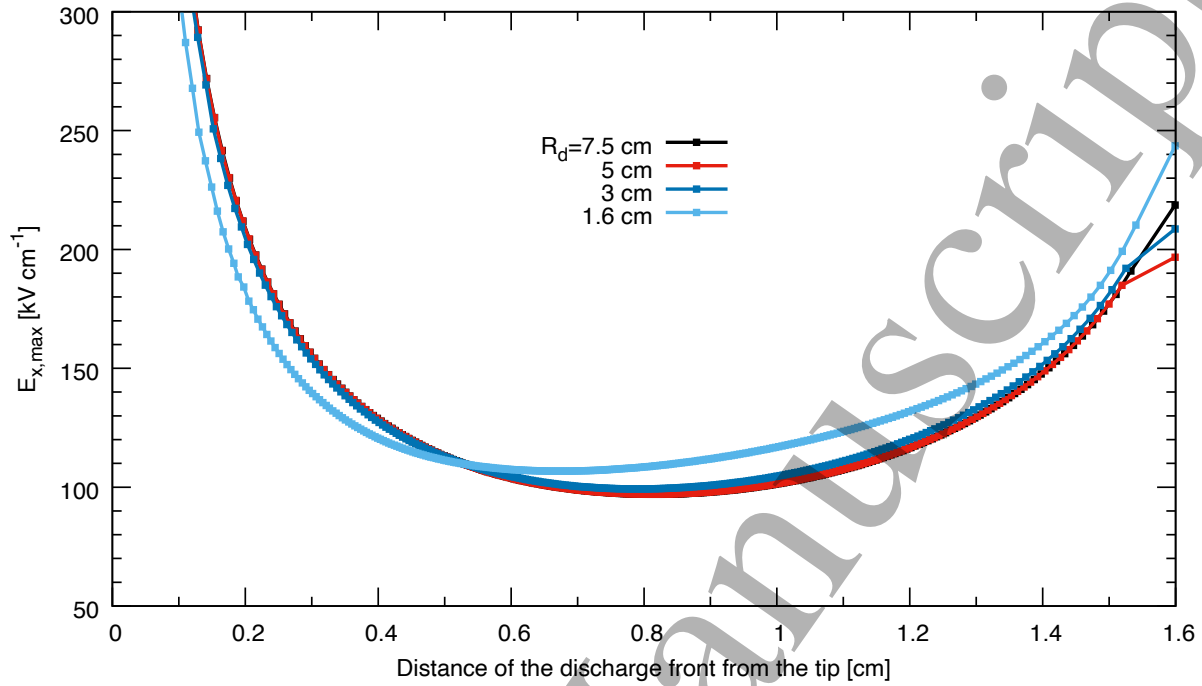


Figure 14. For a DC voltage of 50 kV and a high voltage rod electrode of $R_r = 100 \mu\text{m}$ without a disc holder and for a computational domain of radius $R_d = 7.5, 5, 3$ and 1.6 cm, evolution of (a) $E_{x,\text{max}}$, the maximum absolute value of the electric field on the symmetry axis of the discharge (b) the velocity of the discharge front as a function of the distance of the discharge front from the anode tip.

3.2. Study of the discharge dynamics for an applied voltage of 100 kV with a rise time of 1 ns

In this section, we study the discharge dynamics for a higher applied voltage of 100 kV applied to a point-to-plane geometry with a gap of $d_g=1.6$ cm. To be closer to experimental conditions used to study diffuse nanosecond discharges, the voltage is applied with a voltage rise time of 1 ns. The time evolution of the applied voltage is shown in Figure 15. As already mentioned in section 2, in this section, the point anode electrode is a rod electrode with $R_r = 50 \mu\text{m}$. The radial extension of the computational domain is $R_d = 8.02$ cm. The upper boundary of the computational domain is set at $d_p = 6$ mm and then $L= 2.2$ cm.

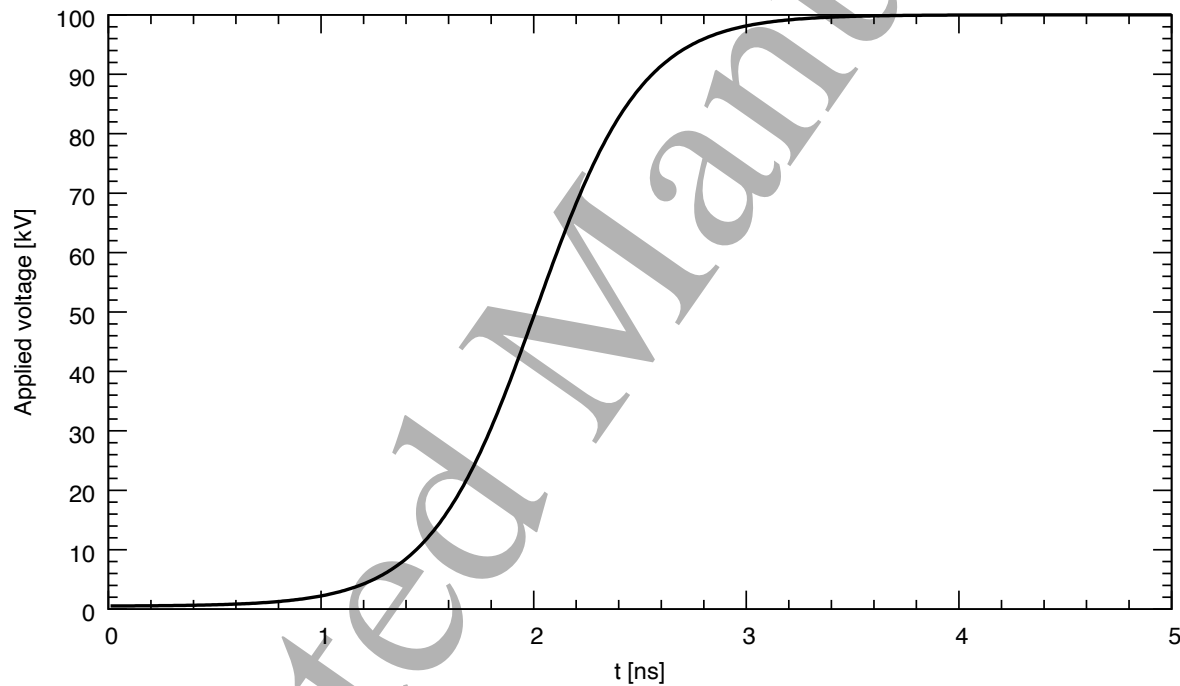


Figure 15. Time evolution of the applied voltage used in Section 3.2

3.2.1. Influence of the presence of a disc holder on the discharge dynamics and characteristics First, we compare the discharge dynamics and structure with and without a disc holder set at $d_p = 6$ mm. The time evolution of the applied voltage on the disc holder is the same as for the rod electrode and is given on Figure 15. The radius of the disc is $R_d = 8.02$ cm. Table 5 gives the values of ignition time τ_i and connection time τ_c to the grounded cathode plane and the radius of the discharge at two locations in the inter-electrode gap at τ_c for the case without and with a disc holder. As observed at lower DC voltages in Section 3.1, the ignition and connection times are shorter without disc holder in comparison to the case with the disc holder. We note

that in both cases, the discharge ignition, propagation and connection to the grounded cathode plane occur during the increase of the applied voltage. Figures 16 and 17 show the cross-sectional views of the absolute value of the electric field and electron density at two instants during the discharge propagation and at the connection time for the case without disc holder, and with disc holder, respectively. As observed at lower DC voltages in section 3.1, the presence of the disc holder has a major influence on the discharge shape and maximum radius at connection. Without disc holder, the discharge has a conical shape at the connection time with a maximum radius of 0.9 cm, whereas with a disc holder, the discharge has a more ellipsoidal shape at connection with a maximum radius of 0.5 cm. As observed for lower DC voltages, in the case without disc holder, a weak cylindrical discharge expands radially around the cylindrical part of the rod electrode. With a disc holder, this parasite radial discharge is completely suppressed.

Figure 18 compares the maximum absolute value of the electric field $E_{x,\max}$ on the symmetry axis and the axial propagation velocity of the discharge front as a function of the axial position of the discharge front in the gap for the case with and without disc holder. As observed at lower DC voltages, we note that the maximum electric field decreases rapidly after ignition. During most of the discharge propagation it remains between 150 and 200 kV cm⁻¹ for the case without disc holder and around 200 kV cm⁻¹ for the case with disc holder. As the discharge front gets closer to the grounded cathode plane, the value of $E_{x,\max}$ increases again. Figure 18 (b) shows that the presence of a disc holder has only a negligible influence on the discharge front propagation velocity. However, on Figure 18 (b) it is interesting to note that with a voltage rise time, after the ignition, the discharge starts propagating much slower than for the lower DC voltages studied in Section 3.1. Discharge front velocities of about 1 cm ns⁻¹ are obtained at $d = 6$ mm and then the discharge front propagation velocity increases up to values larger than 3 cm ns⁻¹ as the discharge front gets closer to the grounded cathode plane.

Table 5. Characteristics of the discharges obtained for a voltage given on Figure 15 applied on a high voltage rod electrode of $R_r = 50 \mu\text{m}$ with a disc holder at $d_p = 6$ mm and without disc holder.

100 kV case	w/o disc holder	with disc holder
Ignition time [ns]	1.37	1.68
Connection time [ns]	2.98	3.30

3.2.2. Time evolution of the electric field for several test points in the gap Recently, measurements of the time evolution of the electric field in a diffuse nanosecond discharge in air at atmospheric pressure in a point-to-plane geometry have been carried out using E-FISH diagnostic (Chng et al., 2019). In Bourdon et al. (2020), temporal evolutions of the electric field on the symmetry axis have been studied at different positions in the

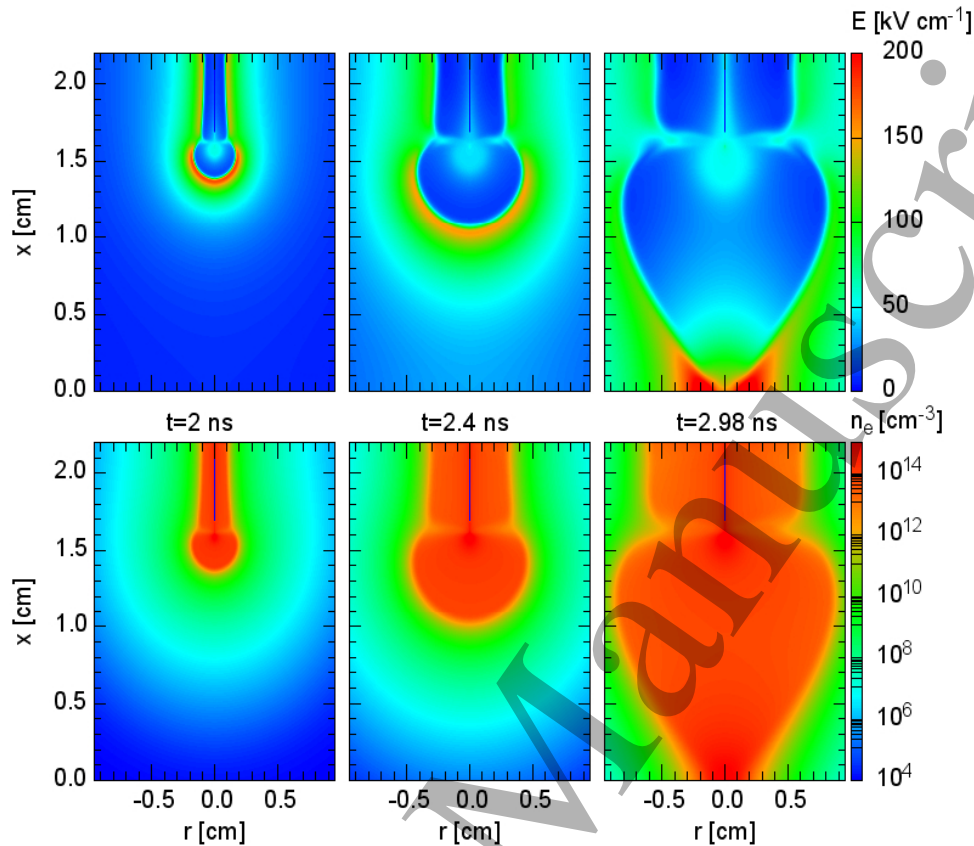


Figure 16. Discharge dynamics for a point-to-plane geometry with a rod electrode with $R_r = 50 \mu\text{m}$ without disc holder and an applied voltage given in Figure 15. Cross-sectional views of the absolute value of the electric field and electron density at $t = 2, 2.4$ and 2.98 ns.

1.6 cm gap for applied voltages varying from 40 to 60 kV with a rise time of 0.5 ns, and for a voltage plateau of 55 kV with rise times in the range 0.5-1.5 ns and a DC voltage case. Recently in Zhu et al. (2021), taking into account the experimental voltage shape (with a rise time of 2.5 ns and a maximum value of 86 kV) and a close-to-experiment shape of the point anode electrode, a quantitative comparison with E-FISH measurements has been done at a test point located at $d = 3$ mm below the tip. A good agreement has been obtained between experiments and simulations. However, it is important to mention, that the accuracy of electric field measurements by E-FISH diagnostic is still under investigation (Lepikhin et al., 2020; Chng et al., 2020).

In this section, we study for the high voltage case of 100 kV studied in the previous section and the case of figure 16 (with a rod electrode with $R_r = 50 \mu\text{m}$ and no disc

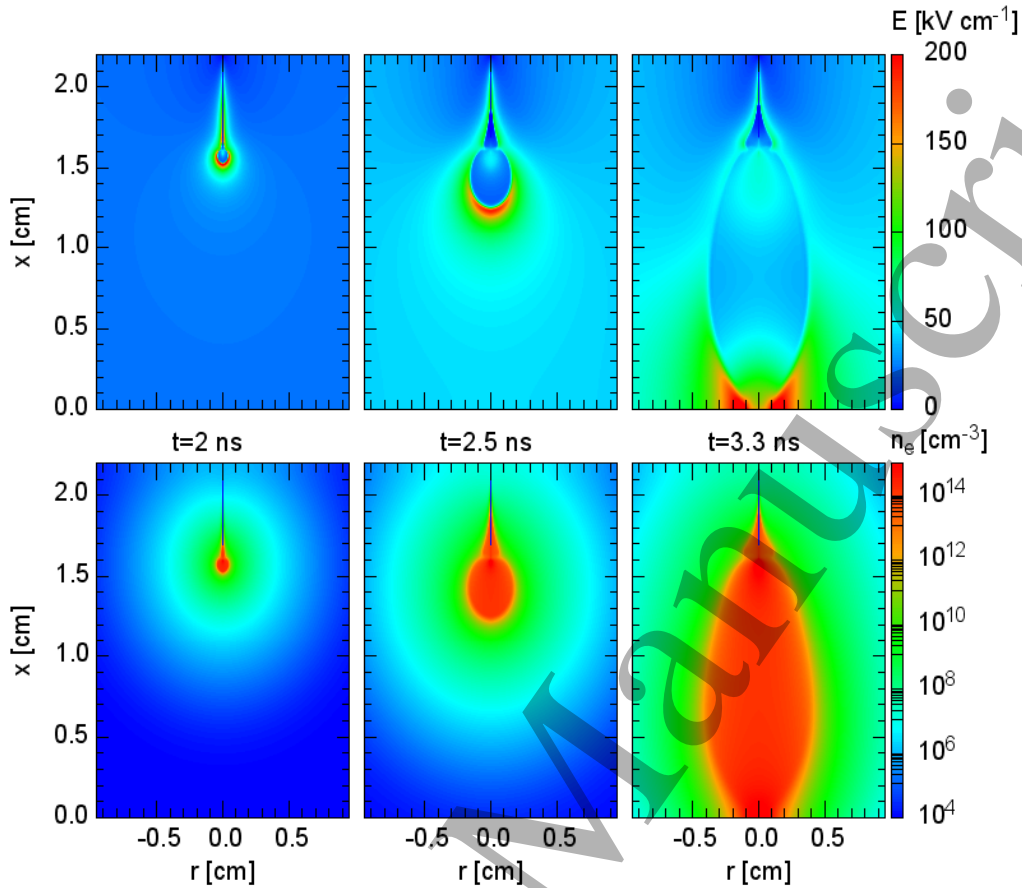
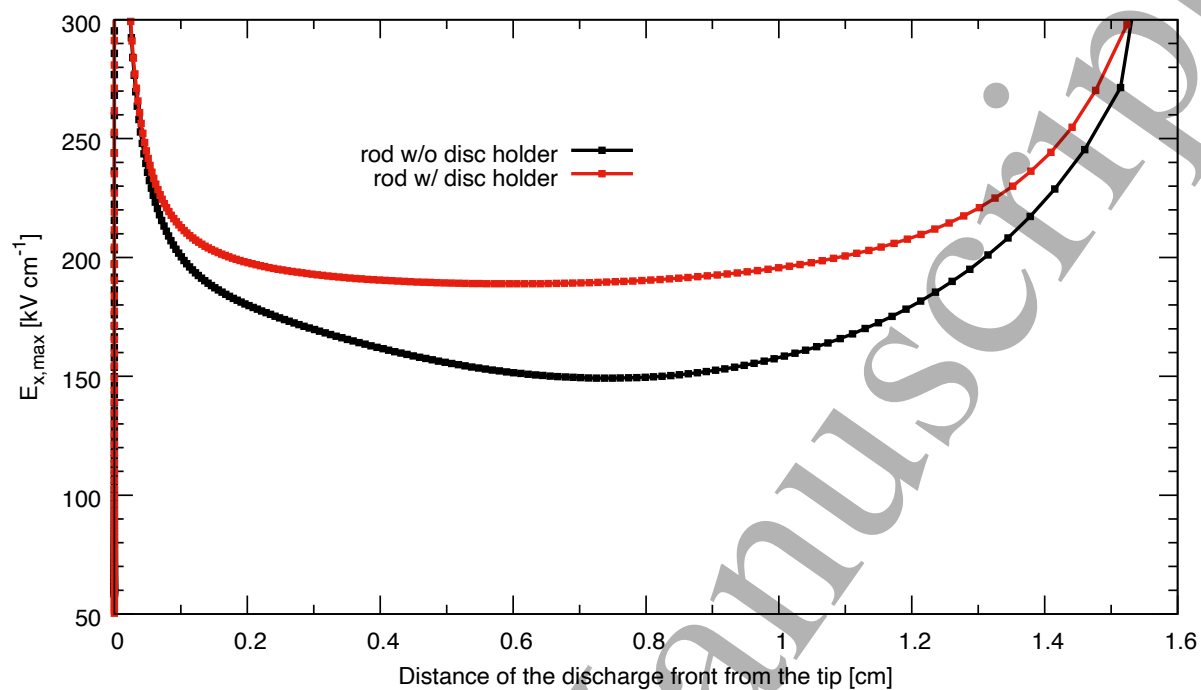


Figure 17. Discharge dynamics for a point-to-plane geometry with a rod electrode with $R_r = 50 \mu\text{m}$ with a disc holder at $d_p = 6 \text{ mm}$ and an applied voltage given in Figure 15, cross-sectional views of the absolute value of the electric field and electron density at $t = 2, 2.5$ and 3.3 ns .

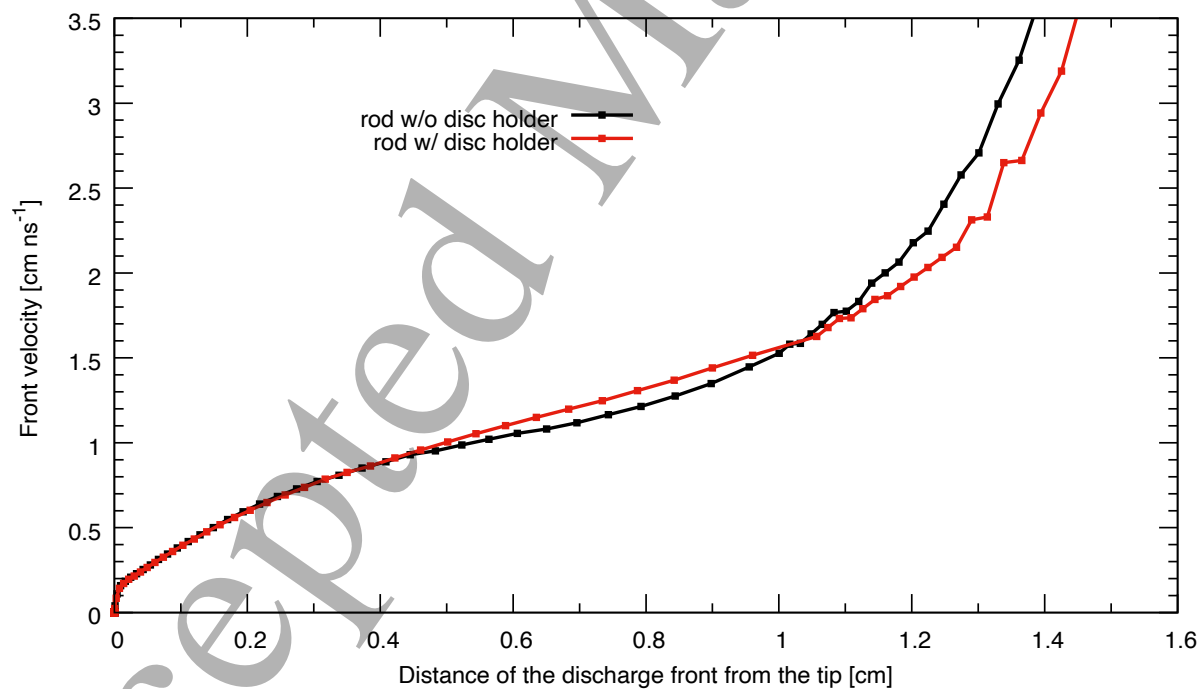
holder) the time evolution of the absolute value of the electric field at different test points in the gap at $d = 2, 5, 8, 11$ and 14 mm with a time sampling of 10 ps . Figure 19 (a) shows that at all positions, a peak of electric field is observed with a time shift corresponding to the axial propagation of the ionization front from the pin to the plane. As already observed in Bourdon et al. (2020) the maximum value of the electric field and the width of the peak of electric field depend on the location of the test point. Figure 19 (b) compares for a test point on the axis close to the tip of the anode at $d = 3 \text{ mm}$, the time evolution of the absolute value of the electric field in the discharge with the Laplacian electric field for the same applied voltage shown in Figure 15. As expected, at early times, the time evolution of the electric field follows the increasing Laplacian field and then as the front approaches the studied test point the value of the electric field becomes higher. After the passage of the discharge front, the electric field decreases

Morphology of positive ionization waves ...

28



(a)



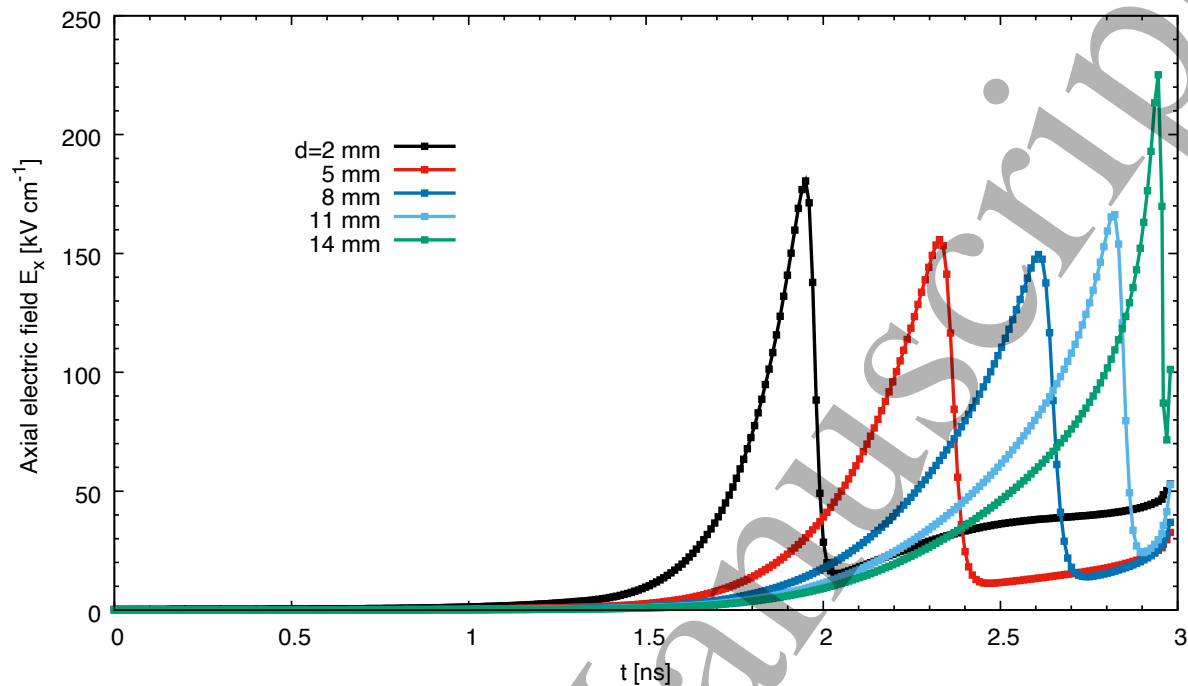
(b)

Figure 18. For a voltage given on Figure 15 applied on a high voltage rod electrode of $R_r = 50 \mu\text{m}$ with a disc holder at $d_p = 6 \text{ mm}$ and without a disc holder, evolution of (a) $E_{x,\text{max}}$, the maximum absolute value of the electric field on the symmetry axis of the discharge, (b) the velocity of the discharge front as a function of the distance of the discharge front from the anode tip.

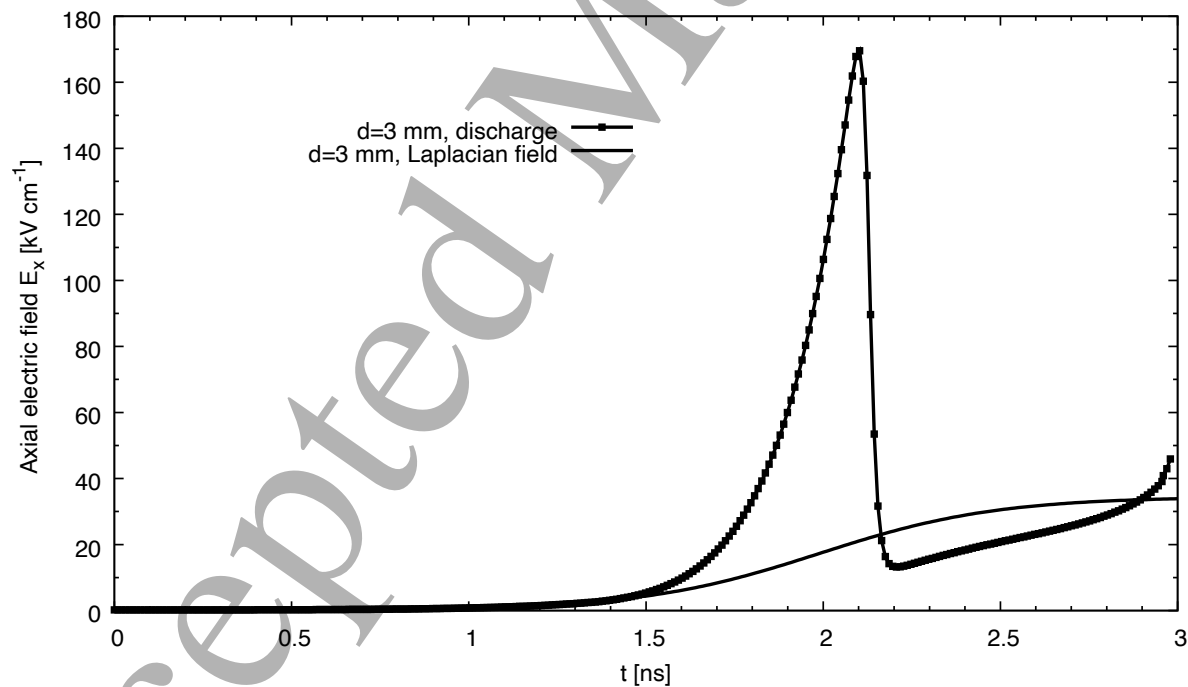
1
2
3 *Morphology of positive ionization waves ...*

29

4 rapidly as observed in experiments (Chng et al., 2019) and in simulations (Bourdon
5 et al., 2020; Zhu et al., 2021). After the peak due to the passage of the discharge front,
6 at lower voltages in Bourdon et al. (2020) where shorter rise times were used to reduce
7 computational times, we have shown that the electric field remains almost constant and
8 starts increasing again only when the discharge front is close to the grounded cathode
9 plane. Conversely, for the high voltage condition studied in the present work, the applied
10 voltage increases during all the propagation of the discharge in the 1.6 cm gap. Close
11 to the anode electrode tip, Figure 19 (b) shows that, after the passage of the ionization
12 front, the electric field increases again rapidly to values higher than the breakdown field
13 as observed in high voltage experiments (Chng et al., 2019) and recently in high voltage
14 simulations (Zhu et al., 2021).
15
16
17
18
19
20
21
22
23
24
25
26
27
28
29
30
31
32
33
34
35
36
37
38
39
40
41
42
43
44
45
46
47
48
49
50
51
52
53
54
55
56
57
58
59
60



(a)



(b)

Figure 19. For a point-to-plane geometry with a rod electrode with $R_r = 50 \mu\text{m}$ without disc holder and an applied voltage given in Figure 15, time evolution of (a) the absolute value of the axial electric field on the symmetry axis of the discharge at different test points located at a distance d from the pin electrode with a time sampling of 10 ps. (b) For $d = 3 \text{ mm}$, comparison of the time evolution of the absolute value of the axial electric field of the discharge on the symmetry axis with the Laplacian electric field on the symmetry axis with a time sampling of 10 ps.

4. Conclusions

In this work, we present a numerical parametric study focused on different characteristics of positive diffuse discharges propagating in a point-to-plane geometry in air at atmospheric pressure: ignition time, connection time at the grounded cathode plane, radius of the discharge at the connection time, evolution of the maximum electric field in the discharge front and velocity of the ionization front during its propagation. First, a reference case is studied consisting in a 1.6 cm gap, a DC voltage of 50 kV and a rod anode with a radius R_r of 100 μm . The influence of the rod radius, presence and position of a disc holder, shape of the high voltage electrode and radial extension of the computational domain are studied. Then, a point-to-plane geometry with a 1.6 cm gap, with a 100 kV voltage applied with a rise time of 1 ns is studied. The point anode electrode is a rod electrode of $R_r = 50 \mu\text{m}$ and the influence of a disc holder of the high voltage point electrode on the discharge characteristics is studied. The principal results of this work can be summarized as follows:

- The radius of curvature of the tip of the high voltage point anode electrode (varied between $R_r = 100$ and $1000 \mu\text{m}$) and its exact shape (rod or hyperbola electrode) are shown to have a negligible influence on the discharge characteristics studied in this work. This parametric numerical study shows that a sharp high voltage point electrode is not mandatory to observe diffuse nanosecond positive ionization waves in point-to-plane geometry in air at atmospheric pressure. It is interesting to note that, in simulations, the use of a blunt electrode allows to reduce numerical constraints on the mesh and time-step. Conversely, in experiments, sharp anode electrodes may be preferred to avoid parasite discharges or jitters at high voltages.
- Conversely, the presence of a disc holder of the point anode electrode or a small radial computational domain lead to a decrease of the maximum discharge radius at the connection time and a change in the discharge shape from a conical to an ellipsoidal shape. It is interesting to note that both the presence of a disc holder or a smaller radial computational domain have a limited impact on the propagation velocity of the discharge front and maximum electric field on the discharge axis.
- In this work, we have considered a simple disc as a holder of the point anode electrode. In simulations, simple shapes of point anode electrodes can be used without any holder, as for example a rod electrode ended by a semi-sphere. For more complex shapes of point anode electrodes, with high applied voltages, parasite radial discharges may be initiated at edges on the surface of the point anode electrode surface or at the boundary of the computational domain. In experiments, holders of electrodes are necessary and can have complex shapes. This study shows the interest to use a large disc (with rounded edges) as holder of the point anode electrode to remove efficiently parasite radial discharges. Therefore, using a large disc as holder of the point anode electrode could ease the quantitative comparison between numerical and experimental studies of diffuse nanosecond discharges at atmospheric pressure.

REFERENCES

32

- For a DC voltage, the propagation velocity of the discharge front is high close to the tip of the anode point and decreases as the discharge propagates in the gap and increases again as the discharge approaches the grounded cathode plane. With a voltage rise time, which duration is about the time for the discharge to cross the gap, the propagation velocity of the discharge front increases monotonically during its propagation.
- For the high applied voltage condition (100 kV) with a rise time of 1 ns, the applied voltage increases during the propagation of the discharge in the 1.6 cm gap. The study of the time evolution of the absolute value of the electric field at different test points on the discharge axis shows an increase and decrease of the electric field, as the ionization front propagates from the high voltage anode electrode to the grounded cathode plane. At a test point close to the anode tip, after the passage of the ionization front, the electric field in the discharge channel is shown to increase rapidly to values higher than the breakdown field before the discharge front connects to the grounded cathode plane.

Finally, in this work, we have used the flexibility of numerical simulations to study separately the effects of several geometrical parameters that can not be decoupled easily in experiments. In this parametric study, a good qualitative agreement on discharge characteristics has been obtained with numerical and experimental data for similar devices. In a future work, we plan to carry out a side-by-side quantitative numerical/experimental comparison study to confirm the impact of the electrode set-up geometry on the characteristics of positive diffuse discharges in atmospheric pressure air.

Acknowledgments

AB is thankful to Drs Tat Loon Chng, David Pai, Olivier Guaitella and Svetlana Starikovskaia for discussions on the experimental study of nanosecond discharges in air at atmospheric pressure. ZB acknowledges support by project LM2018097 funded by the Ministry of Education, Youth and Sports of the Czech Republic. Simulations presented in this work have been performed thanks to the computational resources of the cluster "Hopper" at Ecole Polytechnique.

References

Babaeva, N. Y. and Naidis, G. V. (2016a). Modeling of streamer dynamics in atmospheric-pressure air: Influence of rise time of applied voltage pulse on streamer parameters, *IEEE Transactions on Plasma Science* **44**(6): 899–902.

URL: <https://doi.org/10.1109/TPS.2016.2553081>

Babaeva, N. Y. and Naidis, G. V. (2016b). Simulation of subnanosecond streamers in atmospheric-pressure air: Effects of polarity of applied voltage pulse, *Physics of*

REFERENCES

Plasmas **23**(8): 083527.

URL: <https://doi.org/10.1063/1.4961925>

Babaeva, N. Y. and Naidis, G. V. (2021). Universal nature and specific features of streamers in various dielectric media, *Journal of Physics D: Applied Physics* **54**(22): 223002.

URL: <https://doi.org/10.1088/1361-6463/abe9e0>

Babaeva, N. Y., Naidis, G. V., Tereshonok, D. V. and Son, E. E. (2018). Development of nanosecond discharges in atmospheric pressure air: two competing mechanisms of precursor electrons production, *Journal of Physics D: Applied Physics* **51**(43): 434002.

URL: <https://doi.org/10.1088/1361-6463/aada74>

Bourdon, A., Péchereau, F., Tholin, F. and Bonaventura, Z. (2020). Study of the electric field in a diffuse nanosecond positive ionization wave generated in a pin-to-plane geometry in atmospheric pressure air, *Journal of Physics D: Applied Physics* **54**(7): 075204.

URL: <https://doi.org/10.1088/1361-6463/abbc3a>

Brisset, A., Gazeli, K., Magne, L., Pasquiers, S., Jeanney, P., Marode, E. and Tardiveau, P. (2019). Modification of the electric field distribution in a diffuse streamer-induced discharge under extreme overvoltage, *Plasma Sources Science and Technology* **28**(5): 055016.

URL: <https://doi.org/10.1088/1361-6595/ab1989>

Celestin, S., Bonaventura, Z., Zeghondy, B., Bourdon, A. and Ségur, P. (2009). The use of the ghost fluid method for Poisson's equation to simulate streamer propagation in point-to-plane and point-to-point geometries, *Journal of Physics D: Applied Physics* **42**(6): 065203.

URL: <https://doi.org/10.1088/0022-3727/42/6/065203>

Chen, X., Zhu, Y. and Wu, Y. (2020). Modeling of streamer-to-spark transitions in the first pulse and the post discharge stage, *Plasma Sources Science and Technology* **29**(9): 095006.

URL: <https://doi.org/10.1088/1361-6595/ab8e4e>

Chng, T. L., Brisset, A., Jeanney, P., Starikovskaia, S. M., Adamovich, I. V. and Tardiveau, P. (2019). Electric field evolution in a diffuse ionization wave nanosecond pulse discharge in atmospheric pressure air, *Plasma Sources Science and Technology* **28**(9): 09LT02.

URL: <https://doi.org/10.1088/1361-6595/ab3cfc>

Chng, T. L., Starikovskaia, S. M. and Schanne-Klein, M.-C. (2020). Electric field measurements in plasmas: how focusing strongly distorts the e-FISH signal, *Plasma Sources Science and Technology* **29**(12): 125002.

URL: <https://doi.org/10.1088/1361-6595/abf93>

Höft, H., Becker, M. M., Kolb, J. F. and Huiskamp, T. (2020). Double-propagation mode in short-gap spark discharges driven by HV pulses with sub-ns rise time, *Plasma*

REFERENCES

34

Sources Science and Technology **29**(8): 085002.

URL: <https://doi.org/10.1088/1361-6595/aba112>

Lepikhin, N. D., Luggenhölscher, D. and Czarnetzki, U. (2020). Electric field measurements in a He:N₂ nanosecond pulsed discharge with sub-ns time resolution, *Journal of Physics D: Applied Physics* **54**(5): 055201.

URL: <https://doi.org/10.1088/1361-6463/abbbb4>

Lietz, A. M. and Kushner, M. J. (2018). Electrode configurations in atmospheric pressure plasma jets: production of reactive species, *Plasma Sources Science and Technology* **27**(10): 105020.

URL: <https://doi.org/10.1088/1361-6595/aadf5b>

Marode, E., Dessante, P. and Tardiveau, P. (2016). 2d positive streamer modelling in NTP air under extreme pulse fronts. what about runaway electrons?, *Plasma Sources Science and Technology* **25**(6): 064004.

URL: <https://doi.org/10.1088/0963-0252/25/6/064004>

Naidis, G. V., Tarasenko, V. F., Babaeva, N. Y. and Lomaev, M. I. (2018). Subnanosecond breakdown in high-pressure gases, *Plasma Sources Science and Technology* **27**(1): 013001.

URL: <https://doi.org/10.1088/1361-6595/aaa072>

Pechereau, F. (2013). *Numerical simulation of the interaction of a plasma discharge at atmospheric pressure with dielectric surfaces*, PhD thesis, Ecole Centrale Paris, France.

URL: <https://tel.archives-ouvertes.fr/tel-00978523>

Pechereau, F., Le Delliou, P., Jnsk, J., Tardiveau, P., Pasquiers, S. and Bourdon, A. (2014). Large conical discharge structure of an air discharge at atmospheric pressure in a point-to-plane geometry, *IEEE Transactions on Plasma Science* **42**(10): 2346–2347.

URL: <https://doi.org/10.1109/TPS.2014.2309981>

Tarasenko, V. (2020). Runaway electrons in diffuse gas discharges, *Plasma Sources Science and Technology* **29**(3): 034001.

URL: <https://doi.org/10.1088/1361-6595/ab5c57>

Tarasenko, V. F., Naidis, G. V., Beloplotov, D. V., Kostyrya, I. D. and Babaeva, N. Y. (2018). Formation of wide streamers during a subnanosecond discharge in atmospheric-pressure air, *Plasma Physics Reports* **44**(8): 746–753.

URL: <https://doi.org/10.1134/S1063780X18080081>

Tarasenko, V. F., Naidis, G. V., Beloplotov, D. V., Sorokin, D. A., Lomaev, M. I. and Babaeva, N. Y. (2020). Measuring and modeling streamer velocity at an air discharge in a highly inhomogeneous electric field, *Plasma Physics Reports* **46**(320-327): 034001.

URL: <https://doi.org/10.1134/S1063780X20030113>

Tardiveau, P., Magne, L., Marode, E., Ouaras, K., Jeanney, P. and Bournonville, B. (2016). Sub-nanosecond time resolved light emission study for diffuse discharges

REFERENCES

35

in air under steep high voltage pulses, *Plasma Sources Science and Technology* **25**(5): 054005.

URL: <https://doi.org/10.1088/0963-0252/25/5/054005>

Tardiveau, P., Moreau, N., Bentaleb, S., Postel, C. and Pasquiers, S. (2009). Diffuse mode and diffuse-to-filamentary transition in a high pressure nanosecond scale corona discharge under high voltage, *Journal of Physics D: Applied Physics* **42**(17): 175202.

URL: <https://doi.org/10.1088/0022-3727/42/17/175202>

Xiong, Z., Robert, E., Sarron, V., Pouvesle, J.-M. and Kushner, M. J. (2012). Dynamics of ionization wave splitting and merging of atmospheric-pressure plasmas in branched dielectric tubes and channels, *Journal of Physics D: Applied Physics* **45**(27): 275201.

URL: <https://doi.org/10.1088/0022-3727/45/27/275201>

Zhu, Y., Chen, X., Wu, Y., Hao, J., Ma, X., Lu, P. and Tardiveau, P. (2021). Simulation of the ionization wave discharges: a direct comparison between the fluid model and E-FISH measurements, *Plasma Sources Science and Technology* **30**: 075025.

URL: <http://iopscience.iop.org/article/10.1088/1361-6595/ac0714>

Accepted Manuscript